

Far-from-equilibrium noise heating and laser cooling dynamics in radio-frequency Paul traps

A. Maitra¹, D. Leibfried², D. Ullmo¹, and H. Landa^{3*}

¹*LPTMS, CNRS, Univ. Paris-Sud, Université Paris-Saclay, 91405 Orsay, France*

²*National Institute of Standards and Technology, 325 Broadway, Boulder, Colorado 80305, USA*

³*Institut de Physique Théorique, Université Paris-Saclay, CEA, CNRS, 91191 Gif-sur-Yvette, France*

We study the stochastic dynamics of a particle in a periodically driven potential. For atomic ions trapped in radio-frequency Paul traps, noise heating and laser cooling typically act slowly in comparison with the unperturbed motion. These stochastic processes can be accounted for in terms of a probability distribution defined over the action variables, which would otherwise be conserved within the regular regions of the Hamiltonian phase space. We present a semiclassical theory of low-saturation laser cooling applicable from the limit of low-amplitude motion to large-amplitude motion, accounting fully for the time-dependent and anharmonic trap. We employ our approach to a detailed study of the stochastic dynamics of a single ion, drawing general conclusions regarding the nonequilibrium dynamics of laser-cooled trapped ions. We predict a regime of anharmonic motion in which laser cooling becomes diffusive (i.e., it is equally likely to cool the ion as it is to heat it), and can also turn into effective heating. This implies that a high-energy ion could be easily lost from the trap despite being laser cooled; however, we find that this loss can be counteracted using a laser detuning much larger than Doppler detuning.

I. INTRODUCTION

In the past 50 years, Paul traps have become a major tool for confining charged particles [1]. Certain atomic ion species can be cooled with laser light over more than six orders of magnitude in temperature to the millikelvin regime [2], and with suitable methods further to their quantum ground state, making Paul traps a prominent tool in experiments demonstrating quantum control [3, 4]. However, the nonequilibrium dynamics leading ions from the high energies at creation or after a collision with background gas to the near-equilibrium “Doppler cooling limit” remain poorly understood. Partly, the reason is that Paul traps are based on radio-frequency (rf) electric fields whose interplay with additional external fields that act on the ions poses a theoretical and experimental challenge.

The rapidly oscillating fields of the Paul trap lead to an averaged effective trapping potential with (slower) motion at the characteristic “secular” frequencies. Superimposed on the secular motion is a smaller-amplitude motion at the rf-drive frequency called “micromotion”. Additional, periodic rf-driven motion that is independent of the secular motion amplitude, known as “excess micromotion”, can often be carefully reduced, and we assume here that it can be neglected. The interplay of rf-driven motion and stochastic noise forms a basic example of a system driven far from equilibrium, and has been a concern since the early experiments with trapped ions. The potential in the early Paul traps was typically quadrupolar near the effective potential minimum, leading to linear

equations of motion. In [5] a model for a one-dimensional (1D) periodically driven Mathieu oscillator subject to dissipation and white noise generalized previous works on Brownian motion. The Fokker-Planck (FP) equation for the probability distribution of the particle in phase-space (of position and momentum) admits a Gaussian solution that is periodic with the trap frequency [6–8]. The interplay of the periodic driving with laser cooling was elaborated for a quadrupole trap in some parameter regimes [9], mostly in the final stage of the cooling when the ion settles around the effective potential minimum, and also with excess micromotion [10].

However, above a certain distance from the potential minimum that depends on the trap geometry, the anharmonicity of the potential may start to play an important role. In general, in the absence of stochastic perturbations, the Hamiltonian phase-space for motion in rf Paul traps contains one or more approximately regular (integrable) regions. Within a regular region the motion of the ion is characterized by conserved quantities (the Hamiltonian actions, I_j), whose number is equal to the spatial dimension. Each trajectory is then restricted to rotations in phase-space on a manifold determined by the conserved actions, with the topology of a torus. The time evolution is described by the angle variables $\theta_j(t) = \theta_j(0) + \nu_j t$ with an angular frequency ν_j that is only a function of the actions (and is time-independent), and the initial condition. Due to the micromotion, the invariant tori are periodically modulated in time within the phase-space, at the rf-drive frequency.

Beyond the integrable motion, some phase-space regions may become chaotic, and from some chaotic regions the ion can escape the trap on a very fast timescale [11]. Even for chaotic motion that is bounded, the ion explores

* haggaila@gmail.com

a non-zero volume in phase-space whose dimension is not reduced by conservation laws, and typically does so in an apparently random manner. Thus we can expect that a weak stochastic perturbation within an already chaotic region does not change the evolution qualitatively. In the originally regular region however, a stochastic perturbation breaks the conserved quantities, changing the nature of the motion.

In this work, we consider stochastic heating and laser cooling processes in situations where the ion is initially far from the cooling limit, but within the regular phase-space parts. We strive to answer three main questions: First, due to the widespread use of a time-independent approximation of the rf trap potential (known as the pseudopotential), where can it be employed to obtain a good description of the stochastic dynamics, and where does it fail? Second, how do the stochastic dynamics vary with the amplitude of motion, and does the trap’s anharmonicity introduce qualitative changes in comparison with harmonic motion? If it is possible to answer these two questions in a broad way, we can seek answers to the third and final question about the most advantageous values of laser cooling parameters such as detuning and intensity and also trap parameters such as electrode potentials, to efficiently load ions and to recover the ion to near the cooling limit from collisions with background gas that may put the ion in a state of high kinetic and potential energy.

In Sec. II we approach the task by first transforming the Hamiltonian description of dynamics without stochastic and dissipative events to action-angle variables. We describe the effects of noise and cooling under the assumption that the actions change slowly due to such stochastic perturbations, as compared to the characteristic frequencies ν_j . In this case, one can capture the dynamics by a Fokker-Planck equation where the actions alone suffice to describe the slow stochastic dynamics [12], while the much faster rates of change of θ_j can be eliminated by averaging over these coordinates. The stochastic processes can then be characterized by action-dependent drift and diffusion rates that dynamically reshape a probability distribution over the actions as time goes on. Due to the linearity of the FP equation, different stochastic processes can be accounted for just by adding their coefficients.

In order to approximate the photon scattering during laser cooling, we employ well-established semiclassical simplifying assumptions [2, 9, 13–23]. In Sec. III we treat photon scattering in two approximations: The coarser assumption posits that the excited state of the electron has a lifetime that is negligible on all timescales of the ion dynamics. In this case, each photon is assumed to be absorbed and then spontaneously emitted at the same point in time. We call this the “zero lifetime” limit and it is the limit that Javanainen and Stenholm

called the “heavy particle” limit in their seminal work on laser cooling [14]. The conditions of the zero lifetime limit are violated when the ion’s amplitude of motion grows [15], or when the driven micromotion oscillations are too fast. We remove these restrictions by treating absorption and emission as two events separated in time by intervals that are randomly picked based on the excited state lifetime. We call this the “finite lifetime” limit, and we restrict our treatment to a low saturation of the transition (when the ion spends most of the time in its electronic ground-state). This derivation consistently reduces to the zero lifetime limit when the lifetime of the excited state approaches zero, and our findings agree with previous results in the limits of their scope.

In the remainder of the paper, we apply this framework to study white noise heating and laser cooling with a concrete trap model. In Sec. IV we review the relevant aspects of Hamiltonian motion within Paul traps. In many trap variants [19] there is a region around the effective trap minimum where the potential is approximately a quadrupole, with a symmetry axis along which the motion corresponds to a (time-independent) harmonic oscillator, and in the transverse directions it is described by decoupled Mathieu oscillators. Within a quadrupole potential, the heating and cooling coefficients can be approximated in closed form in some limits [Sec. V]. To go beyond harmonic motion, we focus on a model surface-electrode trap with a five-wire configuration, where it is possible to separate the motion perpendicular to the electrode surface, from the other motional degrees of freedom. We restrict our attention to this 1D motion for which the potential is also strongly anharmonic in a large region, with a detailed characterization of the ranges of validity of the various approximations as a function of the action given in Sec. VI.

A self-contained summary of our results and a discussion of general conclusions is presented in Sec. VII, with Fig. 7 depicting schematically the different regimes of laser cooling. An outlook for possible applications and generalizations is laid out in Sec. VIII. To answer briefly the questions at the outset, for white noise heating we find that the pseudopotential can be safely used, which presents a significant simplification for future studies, while for laser cooling dynamics it turns out to give quantitatively and qualitatively wrong results in most scenarios far from equilibrium. In addition, we find that within a quadrupole potential, the efficiency of laser cooling remains independent of the amplitude of motion in the high action region, while for the strongly anharmonic potential of a surface-electrode trap we find that cooling may become heating, and also change its nature to diffusive at large amplitude motion. This result would be completely lacking in an approximation of the potential as a quadrupole, and even in an approximation using an anharmonic pseudopotential, serving to emphasize the

importance of the interplay of nonlinearity, micromotion and stochastic dynamics in Paul traps. We also present a simple characterization of heating and cooling dynamics at different noise, laser, and trap parameters, and answer the third question posed above, for the studied model five-wire trap. The framework that we provide allows to answer further related questions quantitatively, such as the probability or the time required for the ion to safely arrive at the cooling limit. Moreover, we find that far-from-equilibrium regions are governed by complex dynamics that hold much intrigue by themselves. The presented theory gives a quantitative tool for studying such dynamics and gaining better understanding of the underlying nonequilibrium mechanisms.

II. GENERAL MODEL

A. The Hamiltonian Motion

We consider an ion of mass m and charge e trapped in a general Paul trap, with \vec{r} and $\vec{v} \equiv \dot{\vec{r}}$ being its vector coordinate and velocity in $D = 3$ dimensions, and \vec{p} the canonical momentum. We assume that the Hamiltonian depends quadratically on the momenta, with a potential energy that is a function of the coordinates and is driven periodically in time at rf-drive frequency Ω , so our starting point is the Hamiltonian

$$H_0(\vec{r}, \vec{p}, t) = \frac{1}{2}(\vec{p})^2 + V(\vec{r}, t), \quad V(\vec{r}, t) = V(\vec{r}, t+T), \quad (1)$$

with the potential having period $T = 2\pi/\Omega$ (which can include the particular case where it is time-independent). We also assume that the Hamiltonian H_0 can be approximated as integrable (regular) in some region of phase space, i.e. that D conserved actions exist, and the canonical action-angle coordinates $(\vec{I}, \vec{\theta})$ can be defined and calculated explicitly, at least numerically [11]. A canonical transformation from the real space coordinates is then defined by

$$I_j = \Lambda_j(\vec{r}, \vec{p}, t), \quad \theta_j = \Theta_j(\vec{r}, \vec{p}, t), \quad (2)$$

with the transformation functions Λ_j and Θ_j depending explicitly on time (and being T -periodic), if $V(\vec{r}, t)$ is. In action-angle coordinates, the Hamiltonian H_0 transforms into a Hamiltonian of \vec{I} alone, and the corresponding equations of motion (with an over-dot denoting the time derivative), are

$$\dot{I}_j = 0, \quad \dot{\theta}_j = \nu_j(\vec{I}), \quad (3)$$

$\nu_j(\vec{I})$ being the fundamental frequencies of the motion on the torus defined by fixed actions \vec{I} , which are conserved and thus time-independent.

B. The Fokker-Planck Equation

A trapped ion is subject to different sources of noise and random perturbations [24–27]. In the absence of laser cooling, these typically include collisions of the ion with molecules of the background gas present in the trap, fluctuations of the trap parameters (e.g. Johnson noise on voltages), and fluctuations of ambient electric fields. Stochastic dynamics resulting from such noise can be studied using a probability distribution in phase-space, $P(\vec{r}, \vec{p}, t)$, that evolves under stochastic terms in addition to the motion generated by the trap Hamiltonian, and we follow here the presentation of van Kampen [28]. Noise heating and laser cooling with experimentally relevant parameters (discussed in more detail later) can be modelled by additive, stationary Gaussian white noise (approximating the noise as having no correlation after an infinitesimal time interval) with a nonzero mean. Then the evolution of $P(\vec{r}, \vec{p}, t)$ is described by momentum drift and diffusion coefficients, $B_\alpha(\vec{r}, \vec{p}, t)$ and $D_{\alpha\beta}(\vec{r}, \vec{p}, t)$ respectively, with $\alpha, \beta \in \{x, y, z\}$, using the FP equation

$$\frac{\partial P(\vec{r}, \vec{p}, t)}{\partial t} = \mathcal{L}_0 P - \sum_\alpha \frac{\partial [B_\alpha P]}{\partial p_\alpha} + \frac{1}{2} \sum_{\alpha, \beta} \frac{\partial^2 [D_{\alpha\beta} P]}{\partial p_\alpha \partial p_\beta}, \quad (4)$$

where the Liouvillian \mathcal{L}_0 generates the Hamiltonian flow due to H_0 in phase-space, and is defined by

$$\mathcal{L}_0(\vec{r}, \vec{p}, t) = - \sum_\alpha \frac{p_\alpha}{m} \frac{\partial}{\partial r_\alpha} + \sum_\alpha \frac{\partial V(\vec{r}, t)}{\partial r_\alpha} \frac{\partial}{\partial p_\alpha}. \quad (5)$$

We now transform to the canonical action-angle coordinates $(\vec{I}, \vec{\theta})$ defined in Eq. (2). In these variables the Liouvillian of Eq. (5) reduces to $\mathcal{L}_0(\vec{I}, \vec{\theta}) = - \sum_j \nu_j(\vec{I}) \partial / \partial \theta_j$. Using the formulas of App. D, Eq. (4) will transform to an equation in the new canonical variables. Since the Jacobian of a canonical transformation is equal to 1, the measure of P is unchanged. When the timescale for change in \vec{I} is much longer than the quasi-periods of rotation on the invariant torus, it is possible to approximate $P(\vec{I}, \vec{\theta}, t)$ by its average over the angles, $P(\vec{I}, t)$. In the transformed FP equation (see in general App. D), all terms with derivatives with respect to the angles $\vec{\theta}$ drop out when averaged over the angle. In the case of the rf potential, the averaging is over the entire motion at fixed action, and hence includes also an averaging over the short timescale of the rf potential. This timescale enters through the transformation functions defined in Eq. (2). For any function $\Xi(\vec{I}, \vec{\theta}, t)$ of the phase space which is periodic with the rf-drive frequency,

$$\Xi(\vec{I}, \vec{\theta}, t+T) = \Xi(\vec{I}, \vec{\theta}, t), \quad (6)$$

we define the torus average denoted with an overbar,

$$\bar{\Xi}(\vec{I}) \equiv \frac{1}{T} \int_0^T dt \frac{1}{(2\pi)^D} \int \Xi(\vec{I}, \vec{\theta}, t) d^D \vec{\theta}. \quad (7)$$

After averaging, we obtain the final form of the FP equation in action and time, that can be written in compact form using the probability flux vector \vec{S} whose components are given by

$$S_j(\vec{I}, t) \equiv \Pi_j P - \frac{1}{2} \sum_k \frac{\partial}{\partial I_k} [\Pi_{jk} P], \quad (8)$$

with the FP equation taking the form

$$\begin{aligned} \frac{\partial P(\vec{I}, t)}{\partial t} = & - \sum_j \frac{\partial S_j(\vec{I}, t)}{\partial I_j} = \\ & - \sum_j \frac{\partial}{\partial I_j} [\Pi_j P] + \frac{1}{2} \sum_{j,k} \frac{\partial^2}{\partial I_j \partial I_k} [\Pi_{jk} P], \end{aligned} \quad (9)$$

and the action drift and diffusion coefficients are, respectively,

$$\Pi_j(\vec{I}) = \overline{\sum_{\alpha} B_{\alpha} \frac{\partial \Lambda_j}{\partial p_{\alpha}} + \frac{1}{2} \sum_{\alpha, \beta} D_{\alpha\beta} \frac{\partial^2 \Lambda_j}{\partial p_{\alpha} \partial p_{\beta}}}, \quad (10)$$

$$\Pi_{jk}(\vec{I}) = \overline{\sum_{\alpha, \beta} D_{\alpha\beta} \frac{\partial \Lambda_j}{\partial p_{\alpha}} \frac{\partial \Lambda_k}{\partial p_{\beta}}}. \quad (11)$$

A minimal criterion for the validity of this approximation would be a small relative change in action due to both drift and diffusion, during a cycle of the motion, i.e.,

$$\Pi_j(\vec{I})/\nu_j(\vec{I}) \ll I_j, \quad \Pi_{jk}(\vec{I})/\sqrt{\nu_j(\vec{I})\nu_k(\vec{I})} \ll I_j I_k. \quad (12)$$

It is clear that this adiabatic approximation breaks for $\nu_j(\vec{I}) \rightarrow 0$, i.e. close enough to a separatrix (a trajectory passing through a saddle-point in the potential energy). We return to this point later, where we calculate the stochastic coefficients in the high action regime of a surface trap.

The FP equation can be defined for $I_j > 0$, and is completely posed when boundary and initial conditions are specified. We have a reflecting boundary condition at the origin [$S(I_j = 0, t) = 0$], and an absorbing boundary condition (P itself equals 0) could be enforced at some maximal boundary of \vec{I} (corresponding to the ion escaping the trap). For an initial value problem, a typical initial condition would be e.g. that the ion starts at $t = 0$ with some given distribution (e.g. thermal if it is cooled or arriving from an oven, or power-law after a background-gas collision [29, 30]), or more simply, that it is approximately localized at some action value \vec{I} .

In the following section we consider laser cooling, that allows to counteract the effects of heating in the trap and cool the ion.

III. LASER COOLING

In this section we derive the FP equation describing the process of laser cooling in two different semiclassical

approximations. In Sec. III A we review the well established derivation of the FP equation in the limit that the motion of the ion can be considered as frozen during a photon absorption-emission cycle, stating detailed conditions for the validity of this limit. In Sec. III B we derive the action drift and diffusion coefficients for cooling beyond this limit, by considering the variation of the action due to photon scattering directly.

A. The zero lifetime limit

The ion's valence electron couples the ion's center of mass motion to the electromagnetic field, while making transitions between its ground state and an excited level. We consider the internal states of the ion in a two-level approximation and a monochromatic laser beam in a travelling wave configuration with the following parameters: a laser wavevector \vec{k} and wavenumber $k = |\vec{k}|$, an on-resonance Rabi-frequency Ω_R (with its squared magnitude proportional to the laser intensity), and a laser frequency ω_L detuned by Δ from the resonant electronic transition, whose linewidth (inverse lifetime) is Γ . For each absorption or emission process, the atom suffers a recoil of magnitude $p_r = \hbar k$ which is parallel (antiparallel) to the momentum of the absorbed (emitted) photon, and ensures conservation of the total momentum (\hbar being Planck's constant).

For optical transitions and nonrelativistic ion velocities \vec{v} (much smaller than the speed of light c), the same parameter k can be used for photons resonant with the internal electronic transition, for the detuned laser photons, and for Doppler-shifted photons, i.e.,

$$k = \frac{\omega_L}{c} \approx \frac{\omega_L + \Delta}{c} \approx \frac{\omega_L - \vec{k} \cdot \vec{v}}{c}. \quad (13)$$

A stochastic laser cooling process can be described in a semiclassical approximation by using the FP equation for the probability distribution $P(\vec{r}, \vec{p}, t)$ of the ion's center of mass coordinates alone. When the requirements of the derivation are fulfilled (with the exact conditions discussed below), which can be qualified schematically as the limit of slow enough motion at low amplitude within the pseudopotential approximation, the ion motion can be assumed as frozen during the lifetime of the excited level (in [14] this was called the heavy particle limit). The FP equation in this limit, takes the form of Eq. (4), with two functions that we denote by $B_{\alpha}^z(\vec{p})$ and $D_{\alpha\beta}^z(\vec{p})$.

The vector function $B_{\alpha}^z(\vec{p})$ gives the mean momentum transfer rate due to the radiation pressure force, that acts on the ion as a function of its momentum. The mean momentum gain per cycle is just p_r of the absorbed photon, since the probability to emit a photon in a certain direction is invariant under inversion of the coordinates. The rate of absorption-emission cycles is given by Γ times

the occupation probability of the electron in the excited level, for an ion having momentum \vec{p} in phase-space:

$$\rho_s(\vec{p}) = \frac{s/2}{1 + s + (2\Delta_{\text{eff}}/\Gamma)^2}. \quad (14)$$

Here the saturation parameter s is defined by

$$s = 2(|\Omega_{\text{R}}|/\Gamma)^2, \quad (15)$$

and using the relation of the phase-space momentum to the velocity,

$$\vec{v} = \vec{p}/m, \quad (16)$$

we have that due to the Doppler shift, the detuning of the laser relative to the ion resonance at rest, in the frame of reference of the ion, is

$$\Delta_{\text{eff}} = \Delta - \vec{k} \cdot \vec{v}. \quad (17)$$

Thus $\rho_s(\vec{p})$ describes a Lorentzian with velocity center and velocity half-width given respectively (along the direction of \vec{k}) by

$$v_0 = \Delta/k, \quad \delta v = \Gamma/k. \quad (18)$$

We note that $\rho_s(\vec{p}) < 1/2$, which expresses the saturation of the two-level system for large values of s . With $\hat{k}_\alpha = \vec{k}_\alpha/k$ to specify the direction of the laser wavevector, the momentum change rate is given by

$$B_\alpha^z(\vec{p}) = p_r \hat{k}_\alpha \Gamma \rho_s(\vec{p}). \quad (19)$$

The tensor function $D_{\alpha\beta}^z(\vec{p})$ describes diffusion in momentum due to two sources – the variance in photon absorption, and the spontaneous emission. The second moment of the angular distribution of emitted photons, assumed to be a dipolar transition [13], is for a linearly polarized beam,

$$\mu_{\alpha\beta} = \frac{2}{5} \delta_{\alpha\beta} - \frac{1}{5} \hat{e}_\alpha \hat{e}_\beta, \quad (20)$$

(with \hat{e} the polarization unit vector). The assumed linear polarization can be replaced by circular polarization with just the values of $\mu_{\alpha\beta}$ changing appropriately. This tensor enters as a prefactor in the mean diffusion per cycle due to spontaneous emission, with the cycles proceeding at the rate $\Gamma \rho_s(\vec{p})$. In addition, since the photon absorption events are discrete, there is an independent contribution proportional to the variance of their number per unit time [17]. Assuming uncorrelated Poissonian photon statistics, the variance in the number of absorptions is equal to their mean number, multiplied by a term proportional to $\hat{k}_\alpha \hat{k}_\beta$ accounting for the well-defined direction of momentum transfer, for a total momentum diffusion coefficient

$$D_{\alpha\beta}^z(\vec{p}) = p_r^2 \left(\hat{k}_\alpha \hat{k}_\beta + \mu_{\alpha\beta} \right) \Gamma \rho_s(\vec{p}). \quad (21)$$

Plugging B_α^z of Eq. (19) and $D_{\alpha\beta}^z$ of Eq. (21) into Eqs. (10)-(11) gives the coefficients for the angle-averaged FP equation [Eq. (9)] of cooling in the zero lifetime limit,

$$\Pi_j^z(\vec{I}) = \sum_\alpha B_\alpha^z \frac{\partial \Lambda_j}{\partial p_\alpha} + \frac{1}{2} \sum_{\alpha,\beta} D_{\alpha\beta}^z \frac{\partial^2 \Lambda_j}{\partial p_\alpha \partial p_\beta} \quad (22)$$

$$\Pi_{jk}^z(\vec{I}) = \sum_{\alpha,\beta} D_{\alpha\beta}^z \frac{\partial \Lambda_j}{\partial p_\alpha} \frac{\partial \Lambda_k}{\partial p_\beta}. \quad (23)$$

The derivation of the FP equation [14] assumes an expansion in the following small parameter,

$$k p_r / (m\Gamma) \ll 1 \iff E_{\text{recoil}} = p_r^2 / (2m) \ll \hbar\Gamma, \quad (24)$$

implying that the relative change of $P(\vec{r}, \vec{p}, t)$ in each cycle is small, due to the smallness of the recoil momentum and the associated kinetic energy (E_{recoil}), with respect to the scale determined by the Lorentzian due to the width of the excited level. In addition, the ion's internal (electronic) degrees of freedom have to be adiabatically eliminated. The rate of decay of the excited state (Γ) must be faster than the unperturbed evolution of $P(\vec{r}, \vec{p}, t)$ due to the Liouvillian of Eq. (5), i.e. we require

$$\left| p_\alpha \frac{\partial P}{\partial r_\alpha} \right| \ll \Gamma P, \quad \left| \frac{\partial V}{\partial r_\alpha} \frac{\partial P}{\partial p_\alpha} \right| \ll \Gamma P. \quad (25)$$

For motion within a 3D harmonic potential, assuming a single length scale of variation for P with r_α , determined by the amplitude of the motion in the harmonic limit, the first condition in Eq. (25) amounts to

$$\nu_j \ll \Gamma, \quad (26)$$

known as the unresolved sideband limit. The second condition in Eq. (25) can be written as

$$\max\{\dot{\vec{v}} \cdot \vec{k}\} \ll \Gamma^2, \quad (27)$$

by using the fact that the largest variation of P with momentum results from absorption at the velocity range δv (around v_0), defined in Eq. (18). Thus the condition in Eq. (27) limits the validity of the treatment to low amplitude and low velocity motion in a harmonic oscillator.

For motion in the time dependent rf potential, the averaging over the torus takes care of the rf modulated velocity along the trajectory due to the micromotion, which modifies the instantaneous Doppler shift. Equation (25) still gives conditions for the validity of the current treatment, which must be amended with

$$\Omega/2\pi \ll \Gamma. \quad (28)$$

The conditions that limit the treatment to a small amplitude of motion, and the limitation to the unresolved sideband limit and a small rf frequency in Eq. (28) are very restricting, in particular with state-of-the-art-traps. In the next subsection we develop the semiclassical laser cooling theory in the limit of finite lifetime of the excited electronic state.

B. Laser cooling in the finite lifetime limit

When either of the conditions Eq. (26), Eq. (27) or Eq. (28) do not hold, the ion motion can no longer be considered to be frozen during the absorption-emission cycle, and within the lifetime of the excited level ($1/\Gamma$), the ion's velocity and position may change significantly. A Fokker-Planck equation in energy space has been derived for the large amplitude motion of an ion in a 1D harmonic oscillator potential [15], by making explicit use of harmonic oscillator wavefunctions. We now develop a semiclassical derivation [2, 20, 23], that allows to generalize the results of the previous subsection to the motion in any trap potential, including micromotion, at any amplitude.

The basic principle of this semiclassical derivation is to assume conservation of energy and momentum at each absorption and at each emission event separately, accounting for the ion's centre of mass and internal coordinates together with the photon. Between the absorption and emission, we assume that the ion moves completely classically and is decoupled from the electromagnetic field. It is worth noting that this treatment only alters the description of the emission events, while absorption events are effectively equivalent to their zero-lifetime description. As we will see below, the validity of this treatment requires a low laser intensity, i.e.

$$s \ll 1. \quad (29)$$

With that condition, the probability of an ion to absorb a photon at a given point in phase-space in a small time interval dt equals $\Gamma \rho dt$, with ρ obtained from ρ_s of Eq. (14) by expansion in s ,

$$\rho(\vec{p}) = \frac{s/2}{1 + (2\Delta_{\text{eff}}/\Gamma)^2}, \quad \Delta_{\text{eff}} = \Delta - \vec{k} \cdot \vec{v}, \quad (30)$$

and $\vec{v} = \vec{p}/m$ [Eq. (16)]. The resulting absorption and emission rates are equal on average, even if there are finite delays between these events. A more detailed derivation of the photon absorption probability from the optical Bloch equations will be presented separately in [31] using a Floquet approach, which allows one to improve the accuracy of accounting for the micromotion drive.

Let us consider an ion moving in the trap, and at some arbitrary time t_a when it is at position \vec{r}_a with momentum \vec{p}_a (velocity \vec{v}_a), it absorbs a laser photon of energy $\hbar(\omega_L + \Delta)$. Due to the absorption, the ion's momentum changes by $p_r \hat{k}$, and the electron is excited by the Doppler shifted photon, consistent with the level width Γ and the Lorentzian of Eq. (14), and the condition in Eq. (13). To simplify the notation below, we define the phase-space point

$$Z_a \equiv \{\vec{r}_a, \vec{p}_a, t_a\}. \quad (31)$$

The change in each action I_j due to the absorption is then, to second order in the recoil momentum,

$$\begin{aligned} \delta I_j^{(a)} &= I_j(\vec{r}_a, \vec{p}_a + p_r \hat{k}, t_a) - I_j(\vec{r}_a, \vec{p}_a, t_a) \approx \\ & p_r \sum_{\alpha} \hat{k}_{\alpha} \frac{\partial \Lambda_j(Z_a)}{\partial p_{\alpha}} + \frac{1}{2} p_r^2 \sum_{\alpha, \beta} \hat{k}_{\alpha} \hat{k}_{\beta} \frac{\partial^2 \Lambda_j(Z_a)}{\partial p_{\alpha} \partial p_{\beta}}. \end{aligned} \quad (32)$$

In Eq. (32), $\delta I_j^{(a)}$ is a random variable, that is conditioned on the absorption taking place at Z_a .

Continuing, the ion moves under the influence of the trap and at time t_e reaches the phase space point $\{\vec{r}_e, \vec{p}_e\}$. We take this point to be just the position and momentum that the ion would have reached, if it hadn't absorbed a photon, due to the Hamiltonian evolution from t_a to t_e on the torus of fixed \vec{I} . Hence we neglect the small change for the initial condition at t_a due the ion having made a step $p_r \hat{k}$, which is just the approximation at the basis of the FP approach, that a lot of stochastic events are required to cause a significant change in the action distribution. Now at time t_e the ion spontaneously emits a photon with momentum $\hbar \vec{k} \approx p_r \hat{k}$, where the condition of Eq. (13) has been used. The change in action due to emission occurring at Z_e , of a photon propagating along \hat{k} , and conditioned on absorption at Z_a , is

$$\begin{aligned} \delta I_j^{(e)} &= I_j(\vec{r}_e, \vec{p}_e - p_r \hat{k}, t_e) - I_j(\vec{r}_e, \vec{p}_e, t_e) \approx \\ & - p_r \sum_{\alpha} \hat{k}_{\alpha} \frac{\partial \Lambda_j(Z_e)}{\partial p_{\alpha}} + \frac{1}{2} p_r^2 \sum_{\alpha, \beta} \hat{k}_{\alpha} \hat{k}_{\beta} \frac{\partial^2 \Lambda_j(Z_e)}{\partial p_{\alpha} \partial p_{\beta}}. \end{aligned} \quad (33)$$

Summing Eqs. (32)-(33), the total change to the action given that the absorption occurred at Z_a and the emission at Z_e with the photon going along \hat{k} , is

$$\delta I_j = \delta I_j^{(a)} + \delta I_j^{(e)}. \quad (34)$$

To recap, the ion drift and diffusion in action is due to three sources of randomness: the time and phase-space point of the absorption event, the time and phase-space point of the emission event through decay from the excited level with finite lifetime of $1/\Gamma$, and the direction \hat{k} of the emitted photon. We assume that when coarse-grained over many absorption-emission cycles, the action evolves in small deviations $\delta \vec{I}$ [as in Eq. (34)] about the given torus \vec{I} , due to the accumulation of many small action kicks. The mean action drift and diffusion rates have to be calculated by averaging over multiple emission-absorption cycles using the distribution of the action increments. To a good approximation, the distribution of the sum of many such small action kicks may be taken to be Gaussian due to the central limit theorem. Here we can invoke Eq. (29) and neglect any correlation between the absorption and emission coming from the fact that absorption is impossible while the ion is in the excited level, which can only contribute at order s^2 , and

similarly for stimulated emission processes that can be neglected to lowest order in s . In the following we calculate the first and second moments of the distribution of action kicks, on the torus \vec{I} of the motion.

We start with the random variables of the emission. The mean change in action due to emission is obtained by taking the expectation value of Eq. (33) over the two random variables of emission; the direction of the emitted photons and the phase-space point they are emitted at. The mean over the spherical distribution of $\hat{\kappa}$ is denoted by $\langle \cdot \rangle_{\hat{\kappa}}$, and we have

$$\langle \kappa_\alpha \rangle_{\hat{\kappa}} = 0, \quad \langle \kappa_\alpha \kappa_\beta \rangle_{\hat{\kappa}} = \mu_{\alpha\beta}, \quad (35)$$

in which the term linear in $\hat{\kappa}$ components vanishes since it is reflection-invariant, and the second moment is defined by the tensor $\mu_{\alpha\beta}$ in Eq. (20). The emission time is also a random variable with an exponential distribution for decay from the excited level. Given an absorption that occurred at Z_a , the mean value of any function of phase-space at the time of emission, averaged over the random times of emission, denoted by $\langle \cdot \rangle_\Gamma$, is

$$\langle \Xi(Z_a) \rangle_\Gamma \equiv \int_0^\infty \Gamma e^{-\Gamma t'} \Xi(Z(t_a + t'; Z(t_a) = Z_a)) dt'. \quad (36)$$

The time integral is to be performed along the trajectory $Z(t_a + t')$ in the notation of Eq. (31). Therefore we get for the emission

$$\langle \delta I_j^{(e)} \rangle_{\hat{\kappa}, \Gamma} = \frac{1}{2} p_r^2 \sum_{\alpha, \beta} \mu_{\alpha\beta} \left\langle \frac{\partial^2 \Lambda_j(Z_a)}{\partial p_\alpha \partial p_\beta} \right\rangle_\Gamma. \quad (37)$$

We consider now the effect of the randomness of the absorption event, conditioned so far to occur at the phase-space point and time given by Z_a . As discussed above, the probability of the ion to absorb a photon at a given point in phase-space in a time interval dt equals $\Gamma \rho dt$ [Eq. (30)]. The mean of any random process that depends on absorption at Z_a , calculated for motion during a time interval δt , can be obtained from

$$\langle \Xi \rangle_{\delta t} \equiv \int_0^{\delta t} \Xi(Z_a(t_a)) \Gamma \rho(Z_a(t_a)) dt_a, \quad (38)$$

where δt is the intermediate timescale over which many absorption-emission cycles occur during a large number of rotations on the torus, while the action variation remains small. We assume ergodicity for motion on the torus – i.e. that the average over many photon scattering events during many rotations on the torus, is equal to the average over the torus angles (and the relative micromotion phase), defined in Eq. (7). This ergodicity assumption, over a timescale given by δt is given by writing for the rate of any random process

$$\frac{1}{\delta t} \langle \Xi \rangle_{\delta t} = \Gamma \overline{\rho \Xi}, \quad (39)$$

with the torus average operation

$$\Gamma \overline{\rho \Xi} \equiv \frac{1}{\pi} \int_0^\pi dt \frac{1}{(2\pi)^D} \int \Gamma \rho(Z_a) \Xi(Z_a) d^D \vec{\theta}. \quad (40)$$

Averaging over the absorption events allows us to obtain the FP equation [Eq. (9)] for $P(\vec{I}, t)$, evolving adiabatically at a timescale longer than that for multiple emission-absorption cycles. The first two moments of the action deviations determine the FP equation coefficients [32],

$$\Pi_j^f(\vec{I}) = \langle \delta I_j \rangle / \delta t, \quad \Pi_{jk}^f(\vec{I}) = \langle \delta I_j \delta I_k \rangle / \delta t, \quad (41)$$

where $\langle \cdot \rangle$ denotes the ensemble average to first order in δt , i.e. $\langle \cdot \rangle = \langle \cdot \rangle_{\hat{\kappa}, \Gamma, \delta t}$. Hence we get the FP coefficients

$$\Pi_j^f(\vec{I}) = \Gamma \overline{\rho(Z_a) \langle \delta I_j \rangle_{\hat{\kappa}, \Gamma}}, \quad (42)$$

and

$$\Pi_{jk}^f(\vec{I}) = \Gamma \overline{\rho(Z_a) \langle \delta I_j \delta I_k \rangle_{\hat{\kappa}, \Gamma}}, \quad (43)$$

where we find using Eqs. (34)-(37),

$$\begin{aligned} \langle \delta I_j \rangle_{\hat{\kappa}, \Gamma} &= p_r \sum_\alpha \hat{k}_\alpha \frac{\partial \Lambda_j(Z_a)}{\partial p_\alpha} \\ &+ \frac{1}{2} p_r^2 \sum_{\alpha, \beta} \left[\hat{k}_\alpha \hat{k}_\beta \frac{\partial^2 \Lambda_j(Z_a)}{\partial p_\alpha \partial p_\beta} + \mu_{\alpha\beta} \left\langle \frac{\partial^2 \Lambda_j(Z_a)}{\partial p_\alpha \partial p_\beta} \right\rangle_\Gamma \right], \end{aligned} \quad (44)$$

and to order p_r^2 and s ,

$$\begin{aligned} \langle \delta I_j \delta I_k \rangle_{\hat{\kappa}, \Gamma} &= \\ &p_r^2 \sum_{\alpha, \beta} \left[\hat{k}_\alpha \hat{k}_\beta \frac{\partial \Lambda_j}{\partial p_\alpha} \frac{\partial \Lambda_k}{\partial p_\beta} + \mu_{\alpha\beta} \left\langle \frac{\partial \Lambda_j}{\partial p_\alpha} \frac{\partial \Lambda_k}{\partial p_\beta} \right\rangle_\Gamma \right], \end{aligned} \quad (45)$$

in which, as in Eq. (44), all terms are functions of Z_a , the phase-space point and point where the absorption occurred, on a given torus with actions \vec{I} .

The expressions in Eqs. (42) and (43) hold for an arbitrary rf potential, with the conditions in Eq. (24) and (29) assumed in the derivation, in addition to the adiabaticity conditions of Eq. (12). Assuming that the timescale separation (expressed by these adiabaticity conditions) is justified, the only foreseeable case where the ergodicity assumption of Eq. (39) may fail to hold is the case of one or two decoupled degrees of freedom of the motion which are directed transversally to the laser \vec{k} -vector. Close to such a degenerate case, e.g. when there are two nearly degenerate modes of oscillation, the dynamics have to be treated in more detail (such as in [13], for the case of time-independent harmonic oscillators). The absorption probability taken in Eq. (30) can be improved as in [31] or generalized to a more complicated setup or level-structure.

The difference of the derived action drift and diffusion coefficients to their expressions within the zero lifetime limit [in Eqs. (22)-(23)], lies in the integration over the waiting time distribution for spontaneous emission from the excited electronic state. As a basic consistency check, we see that whenever we can assume an instantaneous absorption-emission cycle and write $\Gamma e^{-\Gamma t'} \approx \delta(t')$ in $\langle \cdot \rangle_\Gamma$ of Eq. (36), the drift and diffusion coefficients reduce in form to those calculated for the zero lifetime limit (and under the assumption $s \ll 1$), whence $\Pi_j^f \rightarrow \Pi_j^z$ and $\Pi_{jk}^f \rightarrow \Pi_{jk}^z$. The cooling coefficients can be further simplified in some limits, and in some cases even integrated in closed form, as we show in the following.

IV. HAMILTONIAN MOTION IN 1D

A. Anharmonic trap potential

For a general anharmonic and time-dependent rf potential $V(\vec{r}, t)$, the motion has to be solved numerically. In [11] the Hamiltonian motion of an ion in the 3D potential of a model surface-electrode trap has been treated for a broad range of parameters, and a range of parameters has been identified wherein the Hamiltonian motion within the full time dependent rf potential is well described by the (time-independent) pseudopotential approximation, with a phase space which is to a high degree regular. To clearly illustrate the main results that we derive here, we present numerical calculations for motion in one spatial dimension, orthogonal to the electrode surface, along the z axis (see Fig. 1). In the five-wire trap in a symmetric configuration (without DC coupling of the radial yz motion), the z motion (which is both time-dependent and nonlinear) decouples exactly for the initial conditions $y = \dot{y} = 0$, for which $y(t) = 0$ at all times. The canonical momentum is $p_z = mv_z$, with the velocity $v_z = \dot{z}$.

From this point on we use nondimensional units, obtained by rescaling the time t by half the micromotion frequency, (we choose $\Omega = 2\pi \times 100$ MHz), and measuring distances using a natural length scale of the problem, the width of each of the two rf electrodes (we take $w = 50 \mu\text{m}$);

$$z \rightarrow z/w, \quad t \rightarrow \Omega t/2. \quad (46)$$

The details of this rescaling (which makes all physical quantities and parameters nondimensional), including the values of the parameters chosen for the numerical calculations, are summarized in App. A. With this rescaling, the rf-drive frequency becomes $\Omega = 2$ and its period $T = \pi$. We also set the ion's mass and charge $m = 1$ and $e = 1$, absorbing their values in the parameters of the nondimensional 1D rf potential, given by

$$V_{\text{rf}}^{\text{1D}}(z, t) = V_0(z) + V_2(z) \cos 2t, \quad (47)$$

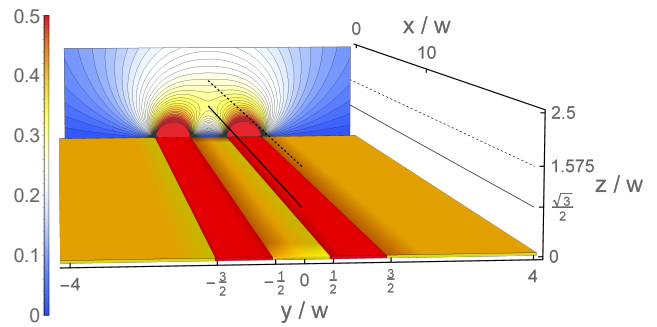


FIG. 1. Layout and rf-potential of the five-wire surface trap. All electrodes lie in the $z = 0$ plane, with the two electrodes connected to the rf-drive shown in red. They are of width w in the y -direction with their center offset by $\pm w$ from $y = 0$. Along the x -direction they are approximated as having an infinite extent. The remainder of the $z = 0$ plane is filled by grounded surfaces, shown in gold. Setting the rf-electrodes to 1 V produces the equipotential lines in the plane $x = 0$ shown as a contour plot in the back of the figure, with the bar legend showing the potential in units of V. The thick solid black line shows the potential minimum line ($z = z_s$) and the thick dashed line shows the saddle-line of the potential.

with

$$V_0(z) = \frac{1}{2} a_z (z - z_s)^2, \quad (48)$$

$$V_2(z) = -\frac{4}{\pi} q_5 \left[\arctan\left(\frac{1}{2z}\right) - \arctan\left(\frac{3}{2z}\right) \right]. \quad (49)$$

The nondimensional parameters a_z and q_5 are determined by the electrode voltages and geometry (and the ion's charge to mass ratio), see Eq. (A6). The potential V_2 of Eq. (49) vanishes at the saddle-point $z = \sqrt{3}/2$, and hence setting $z_s = \sqrt{3}/2 \approx 0.866$ in V_0 of Eq. (48), makes $V_{\text{rf}}^{\text{1D}}(z, t)$ vanish for any value of t at z_s , which then forms the center of the trapping region (see below). The action-angle coordinates (I, θ) , in the integrable approximation of the motion, can be calculated using a stroboscopic map of the motion taken at times $t \pmod{\pi}$, where the action is then related to the phase-space area J bounded within an invariant curve ([11]), by

$$I = J/2\pi. \quad (50)$$

The pseudopotential approximation to Eq. (47) can be obtained by a time dependent canonical transformation from the phase space variables $\{z, p_z, t\}$, to new canonical variables that we denote as ζ for the coordinate and π_ζ for the momentum. The transformation is a perturbative expansion to second order in ν , the ratio of the secular frequency to the rf frequency, assuming that $V_0 \sim \nu^2$ and $V_2 \sim \nu$, and results in a time-independent Hamiltonian, with the time-averaged pseudopotential given by [11]

$$V_{\text{ps}}^{\text{1D}}(\zeta) = a_z \frac{(\zeta - \zeta_s)^2}{2} + q_5^2 \frac{16(3 - 4\zeta^2)^2}{\pi^2(9 + 40\zeta^2 + 16\zeta^4)^2}. \quad (51)$$

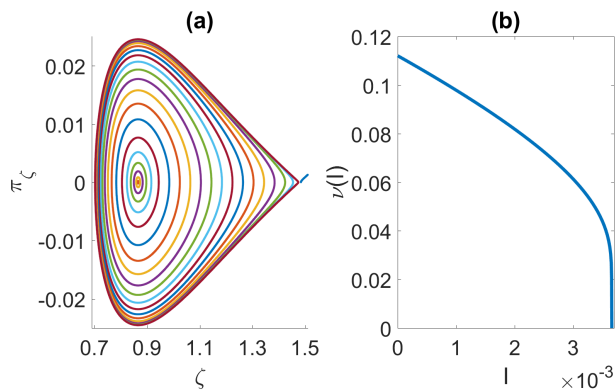


FIG. 2. (a) The phase space of 1D motion perpendicular to the electrodes plane of a five-wire trap, in the pseudopotential approximation [Eq. (51)], with ζ and π_ζ being the coordinate and conjugate momentum in nondimensional units (see Eq. (46) and App. A). The stable fixed point $\zeta_s \approx 0.866$ forms the center of the island, and the unstable fixed point $\zeta_u \approx 1.48$ sits at the “tip” of the bounded part of phase space, with the curve passing through it forming the separatrix. (b) The frequency $\nu(I)$ of rotation around the invariant curves of the phase space, as a function of the action I . We see that $\nu(I=0) = \nu_z \approx 0.112$, and a close examination shows that only very close to the maximal action, which corresponds to the separatrix going through the unstable fixed point, the frequency sharply goes to 0, i.e. $\nu(I) \rightarrow 0$ (this happens within a segment of width $\delta I \lesssim 0.01 \times 10^{-3}$, about $I_{\max} \approx 3.67 \times 10^{-3}$).

The pseudopotential has two fixed points, where the field vanishes. The first point, $\zeta_s = z_s = \sqrt{3}/2 \approx 0.866$, is the stable fixed point at the center of the trap, whose value is independent of the parameters a_z and q_5 , within the pseudopotential (as well as the rf potential). The second point, ζ_u , is an unstable fixed point, a local maximum of the pseudopotential, beyond which the ion escapes the trap (see Fig. 2). The canonical transformation relating the pseudopotential coordinates $\{\zeta, \pi_\zeta\}$ to the original coordinates $\{z, p_z\}$ at every point of phase-space is, to the leading order in the expansion,

$$\zeta = z, \quad \pi_\zeta = p_z + \frac{1}{2} \sin(2t) V_2'(z). \quad (52)$$

For our numerical study, although obtaining the transformation functions of Eq. (2) to the action-angle coordinates within the 1D rf potential is numerically accessible (as demonstrated in [11]), obtaining smooth partial derivatives [required in Eqs. (10)-(11)] is numerically more demanding. Hence we approximate the 1D transformation $I = \Lambda(z, p_z, t)$ using the pseudopotential approximation. Introducing explicit subscripts to denote the form of the potential within which Λ is calculated,

we derive in App. C the approximate relations

$$\begin{aligned} \frac{\partial \Lambda_{\text{rf}}(z, p_z, t)}{\partial p_z} &\approx \frac{\partial \Lambda_{\text{ps}}(\zeta, \pi_\zeta)}{\partial \pi_\zeta} = \frac{\pi_\zeta}{\nu(I)}, \\ \frac{\partial^2 \Lambda_{\text{rf}}(z, p_z, t)}{\partial p_z^2} &\approx \frac{\partial^2 \Lambda_{\text{ps}}(\zeta, \pi_\zeta)}{\partial \pi_\zeta^2} = \frac{1}{\nu(I)} - \frac{\pi_\zeta^2}{\nu(I)^3} \frac{d\nu(I)}{dI}. \end{aligned} \quad (53)$$

The corrections to Eq. (53) for the case of the rf potential will be of a higher (at least second) order in ν , and hence are expected to be quantitatively small.

B. Quadrupole trap potential

As discussed in the introduction, in many cases the Paul trap potential can be approximated as a quadrupole potential around an effective minimum of the trap. Often the motion along a certain direction is nearly decoupled from the other directions due to the symmetry of the trap electrodes. Depending on the nature of the potential in this direction, it can be described by a time-dependent Mathieu oscillator if the potential is periodically modulated in time, or a harmonic oscillator if the potential is static (time-independent). For concreteness, we consider the idealized five-wire surface electrode trap introduced in Sec. IV A in the following. This geometry naturally implements the harmonic oscillator along the trap axis of symmetry (x , not considered here), and Mathieu oscillators in the transverse plane. For simplicity we here consider motion along one direction (denoted by z) and compare a Mathieu oscillator and a harmonic oscillator with identical secular frequencies.

The leading order expansion of $V_{\text{rf}}^{1\text{D}}$ of Eq. (47) about z_s gives the Mathieu oscillator potential

$$V_{\text{rf}}^{1\text{D}} \rightarrow V_{\text{M.o.}}^{1\text{D}} \equiv \frac{1}{2} (a_z - 2q_z \cos 2t) z^2, \quad (54)$$

that results in a linear equation of motion, with the Mathieu parameter $q_z = 2q_5/(\sqrt{3}\pi)$. The nondimensional secular frequency of oscillation in the trap (also called the characteristic exponent), $\nu_z(a_z, q_z)$, can be approximated in the limit $a_z, q_z^2 \ll 1$ by

$$\nu_z \approx \sqrt{a_z + q_z^2/2}. \quad (55)$$

The transformation functions between real space coordinates and action-angle variables for Mathieu oscillators can be obtained exactly as presented separately [31]. Here we use a leading order approximation, obtained using Eq. (52), which for the Mathieu oscillator reduces to

$$\zeta \rightarrow z, \quad \pi_\zeta \rightarrow p_z - q_z \sin(2t) z. \quad (56)$$

The expansion of $V_{\text{ps}}^{1\text{D}}$ of Eq. (51) about ζ_s gives the harmonic oscillator potential,

$$V_{\text{h.o.}}^{1\text{D}} \equiv \frac{1}{2} \nu_z^2 \zeta^2, \quad (57)$$

whose frequency coincides with ν_z appearing in Eq. (55). The action is related to the energy E by $I \rightarrow E/\nu_z$ and the (inverse) action-angle transformation is

$$\zeta \rightarrow \sqrt{\frac{2I}{\nu_z}} \cos \theta, \quad \pi_\zeta \rightarrow -\sqrt{2I\nu_z} \sin \theta, \quad (58)$$

where the angle is defined by

$$\theta = \nu_z t + \phi, \quad (59)$$

with ϕ determined by the initial conditions. The motion lies on an ellipse in phase space with area $J = 2\pi I$, evolving clockwise in the (ζ, π_ζ) plane. The approximation of Eq. (53) then reduces to

$$\frac{\partial \Lambda_{\text{M.o.}}}{\partial p_z} \approx \frac{\partial \Lambda_{\text{h.o.}}}{\partial p_z}, \quad \frac{\partial^2 \Lambda_{\text{M.o.}}}{\partial p_z^2} \approx \frac{\partial^2 \Lambda_{\text{h.o.}}}{\partial p_z^2}, \quad (60)$$

with the simple formulae for the harmonic oscillator,

$$\frac{\partial \Lambda_{\text{h.o.}}}{\partial p_z} = \frac{\pi_\zeta}{\nu_z}, \quad \frac{\partial^2 \Lambda_{\text{h.o.}}}{\partial p_z^2} = \frac{1}{\nu_z}. \quad (61)$$

Throughout the numerical simulations in this work we have compared the results obtained by using the approximation given in Eq. (60), to the exact value of $\partial \Lambda_{\text{M.o.}}/\partial p_z$ (obtained using [33] and presented separately [31]), and the difference is quantitatively very small (given by approximately q_z^2).

V. ANALYTIC LIMITS OF STOCHASTIC MOTION IN 1D

In this section we consider the form of the action drift and diffusion coefficients that enter the FP equation describing different heating and cooling processes in 1D. We summarize here all of the analytic results that apply to 1D motion, with a simplified notation. In some of the cases, the averaging of the FP coefficients can be carried out explicitly and closed form expressions are presented in the following. We postpone however a detailed discussion of the results to the following sections (to Sec. VI where all figures are presented together and the different dynamics compared, and to Sec. VIII which contains a summary and an outlook). For the 1D motion the general FP equation in action [Eq. (9)], takes the simplified form

$$\frac{\partial P(I, t)}{\partial t} = -\frac{\partial S(I, t)}{\partial I} = -\frac{\partial}{\partial I} [\Pi_I P] + \frac{1}{2} \frac{\partial^2}{\partial I^2} [\Pi_{II} P]. \quad (62)$$

We can gain insight into the cooling dynamics by using the drift and diffusion rates at any value of I to define (respectively) a drift timescale $\tau_{\text{drift}}(I)$ and a diffusion

timescale $\tau_{\text{diffuse}}(I)$, and form a nondimensional coefficient that measures the cooling efficiency,

$$\varepsilon(I) \equiv \frac{\Pi_I I}{\Pi_{II}} \propto \frac{\tau_{\text{diffuse}}(I)}{\tau_{\text{drift}}(I)}. \quad (63)$$

The sign of ε depends on the sign of the drift coefficient, and is negative when the laser is cooling the ion (in the mean), while if it is positive, the laser effectively heats the ion. A large value of $|\varepsilon|$ signifies that the drift time is much shorter than the time it takes to diffuse a similar range of action, so that for $\varepsilon \ll -1$ the cooling is efficient. In contrast, for $-1 \lesssim \varepsilon \lesssim 1$ the width of the ion's distribution in I grows faster than its mean drifts. Diffusive motion has no directionality, and may equally well lead the ion down or up in action.

For completeness we note that a steady-state of the Eq. (62) [assuming one exists], can be obtained in terms of the FP coefficients, with a distribution which can be thermal-like (exponential) or very different, as will be discussed in a future publication.

A. White Noise Heating in 1D

For an ion subject to position-independent Gaussian white noise, the 1D action drift and diffusion coefficients are

$$\Pi_I^{\text{W}}(I) = D \frac{\partial^2 \Lambda}{\partial p_z^2}, \quad \Pi_{II}^{\text{W}}(I) = 2D \left(\frac{\partial \Lambda}{\partial p_z} \right)^2, \quad (64)$$

with D being the nondimensional diffusion coefficient. White noise can be thought of as being produced by a reservoir at infinite temperature and causes only heating. In this case there is no steady-state distribution.

For the harmonic oscillator $V_{\text{h.o.}}^{\text{1D}}$ of Eq. (57), we have

$$\Pi_I^{\text{W}} \rightarrow D/\nu_z, \quad \Pi_{II}^{\text{W}} \rightarrow 2DI/\nu_z, \quad (65)$$

and for the quadrupole potential $V_{\text{M.o.}}^{\text{1D}}$, the Mathieu oscillator of Eq. (54), within the approximation of Eqs. (52)-(53), the result is identical to the harmonic oscillator, neglecting as discussed above, a small correction of approximately q_z^2 . In addition, as we confirm by numerical simulations, due to the form of Eq. (64) and by using Eq. (53) explicitly, also for motion within an anharmonic Paul trap potential, the effect of the micromotion is averaged out and can be neglected.

In the case of heating within a quadrupole potential, a solution by separation of variables, with a reflecting boundary condition at $I = 0$, and the initial condition $P(I, t = 0) = \delta(I)$ (the ion starting at the origin), can be integrated in closed form. As can be verified directly by substitution it results in the time-dependent distribution

$$P(I, t) = \frac{\nu_z}{Dt} \exp \left\{ -\frac{\nu_z}{Dt} I \right\}, \quad (66)$$

with the expected mean torus drift

$$\langle I(t) \rangle = Dt/\nu_z. \quad (67)$$

For the harmonic oscillator (for which energy is conserved), this is equivalent to the mean heating rate in energy $\langle \dot{E} \rangle = \langle \nu_z \dot{I} \rangle = D$.

In the following section we study quantitatively the laser cooling process in the trap, and we will compare the heating rate values calculated for white noise with the laser-induced cooling rates.

B. Laser cooling in a general 1D potential

For motion in 1D, the FP coefficients of Eqs. (22)-(23) for cooling in the zero lifetime limit with the decay occurring at the phase-space point of the absorption, are

$$\Pi_I^z = \Gamma \rho_s \overline{\left[p_r \frac{\partial \Lambda}{\partial p_z} + \frac{1}{2} p_r^2 (1 + \mu) \frac{\partial^2 \Lambda}{\partial p_z^2} \right]}, \quad (68)$$

$$\Pi_{II}^z = \Gamma p_r^2 (1 + \mu) \rho_s \overline{\left(\frac{\partial \Lambda}{\partial p_z} \right)^2}, \quad (69)$$

with $\mu \equiv \mu_{zz}$ of Eq. (20). All terms in the right hand side of the equations above are functions of $Z_a = \{z, p_z, t\}$, the phase-position, momentum and time where the absorption occurred, that is averaged on a given torus by the definition in Eq. (7).

For the finite lifetime case, Eqs. (42)-(43) become

$$\Pi_I^f = \Gamma \rho \overline{\left[p_r \frac{\partial \Lambda}{\partial p_z} + \frac{1}{2} p_r^2 \left(\frac{\partial^2 \Lambda}{\partial p_z^2} + \mu \left\langle \frac{\partial^2 \Lambda}{\partial p_z^2} \right\rangle_\Gamma \right) \right]}, \quad (70)$$

$$\Pi_{II}^f = \Gamma p_r^2 \rho \overline{\left[\left(\frac{\partial \Lambda}{\partial p_z} \right)^2 + \mu \left\langle \left(\frac{\partial \Lambda}{\partial p_z} \right)^2 \right\rangle_\Gamma \right]}, \quad (71)$$

with the emission point Z_e averaged by the integration of the waiting time distribution $\langle \cdot \rangle_\Gamma$ defined in Eq. (36).

The dynamics of the laser cooling around a given torus are determined both by the form of the potential (that depends on the displacement of the ion), and by the velocity, as compared to a relevant scale determined by the laser parameters. The limits of low velocity and of high velocity lend themselves to expansion in a suitable, distinct small parameter. For motion in a quadrupole potential this allows a simplification of the FP coefficients, explored in the following two subsections for 1D motion.

C. The linear limit of laser cooling

In a Paul trap whose potential reduces to a quadrupole at its center (as in linear Paul traps and surface-electrode traps, but not in higher multipole traps), and in the absence of excess micromotion, the ion velocities can be

assumed to be small at the center of the trap. These two conditions define a specific limit of the cooling, that can be analyzed analytically. The Lorentzian can be linearized in the velocity, with the coefficients written in a well-known form [13, 19], for $s \ll 1$,

$$p_r \Gamma \rho(p_z) \approx F_r + \gamma v_z, \quad (72)$$

with

$$F_r = \frac{p_r \Gamma s/2}{1 + (2\Delta/\Gamma)^2}, \quad \gamma = \frac{4k p_r s \Delta/\Gamma}{[1 + (2\Delta/\Gamma)^2]^2}. \quad (73)$$

Here F_r gives a mean radiation force (for $p_z = 0$), and γ/m (with $m = 1$ in the rescaled units) is the damping rate. This linearization is valid if

$$k v_z \ll [\Gamma^2 + 4\Delta^2]/(8|\Delta|), \quad (74)$$

which can be rewritten in terms of the action,

$$I \ll I_{\text{linear}} = \left(\frac{\Gamma^2 + 4\Delta^2}{8k\Delta} \right)^2 \frac{1}{2\nu_z}. \quad (75)$$

In this approximation, since the Lorentzian is linear in the momentum, and the partial derivatives of the action are (at most) linear in the momentum (for a quadrupole potential), the resulting cooling coefficients are at most linear in the actions. For the harmonic oscillator the integration in closed form of the action drift and diffusion coefficients is straightforward and we can write

$$\Pi_I^1 = \gamma I + h_z/2, \quad \Pi_{II}^1 = h_z I, \quad (76)$$

with

$$h_z = p_r F_r (1 + \mu)/\nu_z. \quad (77)$$

Then the linear limit of the cooling is characterized by a thermal equilibrium-like distribution (for $\Delta < 0$), determined by the balance of momentum dissipation and diffusive heating. The mean value and standard deviation of the action, $\langle I \rangle = \sqrt{\langle (I - \langle I \rangle)^2 \rangle} = I_{\text{limit}}$, reads

$$I_{\text{limit}} \equiv \hbar \frac{\Gamma}{8\nu_z} (1 + \mu) \left[\frac{\Gamma}{2|\Delta|} + \frac{2|\Delta|}{\Gamma} \right]. \quad (78)$$

The expression above is identical to the known results for the thermal distribution of an ion cooled within a 1D harmonic oscillator [19], in the limit of $s \ll 1$. Remarkably we find in the numerical simulations presented in Sec. VIA that the results for the Mathieu oscillator are nearly identical [up to the accuracy of Eq. (60), neglecting a correction of approximately q_z^2]. Analytic expressions for the coefficients can be obtained for general 3D motion in a Mathieu oscillator potential, which is beyond the scope of the current work and will be presented separately.

D. The (quadrupole) fast particle limit of laser cooling

A second regime of motion that allows a simplification of the expressions of the action coefficients of laser cooling is the (quadrupole) fast particle limit, where the motion is of a large enough amplitude, within a quadrupole potential. In this case, the ion velocity creates a large Doppler shift which tunes the cooling light *out* of the resonance with the ion for most of the time. In a harmonic motion the measure on the invariant torus where the light field is resonant with the ion, bounded within the strip $\vec{k}\cdot\vec{v} = v_0 \pm \delta v$ [the resonance has width δv around v_0 , defined in Eq. (18)], is independent of the action, and its fraction of the total torus measure decreases with I . Within the tori averages, the contribution from the resonance region decreases accordingly, while the contribution from the rest of the torus increases with I due to the tails of the Lorentzian distribution, which eventually dominate the torus averages.

The cooling and diffusion terms within the fast particle limit are derived in App. B on the basis of an expansion for the Lorentzian expression of the excited state occupation. For the case that the laser propagates along one of the principal axes of the motion [here, $\vec{k} = k\hat{z}$], and if in addition the motion is described by a harmonic oscillator [Eq. (58)], the fast particle limit expressed in terms of the action is

$$I \gg I_{\text{fast}} \equiv \frac{\max\{4\Delta^2, \Gamma^2/4\}}{\nu_z k^2/2}. \quad (79)$$

We have integrated the drift and diffusion coefficients in closed form [Eqs. (B3)-(B4)], and a basic property of the coefficients in this limit is their action dependence [15],

$$\Pi_I^{\text{f.p.}} \propto -1/\sqrt{I}, \quad \Pi_I^{\text{f.p.}} \propto \sqrt{I}. \quad (80)$$

We note that the zero lifetime treatment for a harmonic oscillator gives the same cooling rate in terms of the energy (which has been used, e.g., in [20, 23]), but results in a constant (independent of I) diffusion term [Eq. (B5)], which is incorrect since Eq. (80) shows a scaling $\propto \sqrt{I}$.

As discussed in Sec. VI B, for motion within a Mathieu oscillator potential we find by numerical integration that the action dependence is identical in form [obeying Eq. (80)], with the prefactors depending on the Mathieu oscillator parameters. The implications of these functional relations are discussed in Sec. VI B, and the deviations from them for motion in the anharmonic rf potential, in Sec. VI C.

VI. A STUDY OF HEATING AND COOLING IN 1D

In this section we present a detailed numerical study of heating and cooling processes for ion motion in 1D. We

Potential is	Time-independent	Time-dependent
Quadrupole	Harmonic oscillator (h.o.)	Mathieu oscillator (M.o.)
Anharmonic	Pseudopotential (ps)	Rf potential (rf)

TABLE I. The four different types of trap potentials, summarized with their acronyms used in the figures to follow and in the equations. Depending on the Paul trap type, along each of its spatial dimensions the potential can be quadrupole or anharmonic, and either static or periodically driven.

Notation	Definition
Π_I^w, Π_{II}^w	Position-independent additive <u>white</u> noise Eq. (64)
Π_I^z, Π_{II}^z	Laser cooling in the zero lifetime (heavy particle) limit Eqs. (68)-(69)
Π_I^f, Π_{II}^f	Laser cooling in the <u>finite</u> lifetime limit Eqs. (70)-(71)
$\Pi_I^{\text{f.p.}}, \Pi_{II}^{\text{f.p.}}$	Laser cooling in the <u>fast</u> <u>particle</u> limit Eq. (80)
Π_I^l, Π_{II}^l	Laser cooling in the <u>linear</u> limit Eq. (76)

TABLE II. The different types of action drift and diffusion coefficients, used in figures to follow and in the equations.

compare the results for motion within the four realizations of a trap potential described in Sec. IV. For reference, these are summarized in Table I, together with their acronyms (used in the figures and equations). In Table II we summarize the notation indicating the action drift and diffusion coefficients that correspond to the different physical processes and parameter regimes, presented in the figures that follow in this section and the equations used to calculate them..

For most of the calculations in the following (except where explicitly stated otherwise), we set the laser detuning to the Doppler detuning, with a low saturation parameter,

$$\Delta = -\Gamma/2, \quad s = 0.01. \quad (81)$$

For the chosen ${}^9\text{Be}^+$ ion and in the nondimensional units introduced in Eq. (46), we have $\Gamma = 0.38$, see App. A for details of the laser (and trap) parameters. Motional heating is represented by a white noise rate, and we choose a representative value of the nondimensional diffusion coefficient D that corresponds to a heating rate in units of motional quanta per second near the effective potential minimum (see App. A), of

$$\dot{n} = 0.1 \text{ ms}^{-1}, \quad (82)$$

except in Fig. 3.

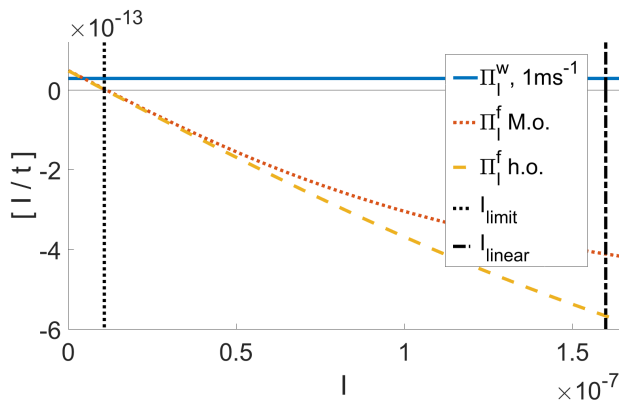


FIG. 3. The action drift coefficients for laser cooling [Π_I^f , Eq. (70)], and for white noise heating [Π_I^w , Eq. (64)] in nondimensional units, for low amplitude motion. In this regime the rf potential is accurately approximated by its Mathieu oscillator limit. The trap parameters, laser parameters, and heating rate parameters are given in App. A. For this figure only, we have set the saturation parameter to $s = 0.001$, and the heating rate, in terms of quanta per unit time, to $\dot{n} = 1 \text{ ms}^{-1}$. The vertical lines show I_{linear} , the border of validity of the linear limit of the cooling [Eq. (75)], and the action at the Doppler cooling limit, I_{limit} [Eq. (78)]. It can be seen how the Mathieu and the harmonic oscillator (of the same secular frequency) converge for $I \ll I_{\text{linear}}$ to the same curve, and for both curves the drift vanishes as $I = I_{\text{limit}}$. See the text for a discussion of the competing effects of heating $\Pi_I^w \propto D$ and cooling $\Pi_I^f \propto s$.

A. Cooling in the low velocity regime

Although ions are cooled from high-amplitude motion towards low amplitude, we present our detailed study of laser cooling starting with low amplitude motion with $I \lesssim I_{\text{linear}}$ [defined in Eq. (75)]. The action drift coefficient Π_I^f is composed of the sum of the absorption term (linear in p_r), and the emission term ($\propto p_r^2$). The dynamics is determined by the competition of the two terms, since the first is negative (for $\Delta < 0$) and the second is positive, resulting from the diffusion in phase-space. The action value for which $\Pi_I^f = 0$ (and has a negative slope), is where the mean drift balances, with the ion being heated (by momentum diffusion) for lower values of I , and cooled back from higher I . Figure 3 shows that for $I \ll I_{\text{linear}}$, both the Mathieu and harmonic oscillator drift rates converge to the same curve, reducing in this limit to the expression of Eq. (76). The numerically calculated zero-crossing for both the harmonic oscillator and the Mathieu oscillator coincide very closely with the (thermal-equilibrium-like) limit of Eq. (78). The crossing points are independent of s (in the limit $s \ll 1$) but the slope is proportional to s , which is important if heating of a comparable rate is present. The action drift rate resulting from white noise heating at a rate of 1 quan-

tum per millisecond (10 times more than in the following figures, a value that can be considered as high but not excessive in current state-of-the-art traps), is shown for comparison. Such a high heating rate will shift the cooling limit to a action value where the sum $\Pi_I^w + \Pi_I^f$ crosses 0, and increase the final mean value of the action (with these parameters to $\sim 2I_{\text{limit}}$). However, the saturation parameter in this figure is taken to be $s = 0.001$, much lower than what is typically used in experiments. Since the heating drift rate scales linearly with $D \propto \dot{n}$, and the cooling rate scales linearly with the intensity $\propto s$ (for $s \ll 1$), the cooling limit is quite insensitive to heating at this order of magnitude. For $I \gtrsim 0.5 \times 10^{-7}$, i.e. where the condition $I \ll I_{\text{linear}}$ no longer holds, the Mathieu and harmonic oscillator cooling rates begin to deviate (with the former being smaller).

B. Cooling in the high velocity regime of a quadrupole potential

The Mathieu and harmonic oscillator cooling rates, although deviating from each other for $I \gtrsim I_{\text{linear}}$, both show an asymptotic slow approach towards zero at high action. The numerically calculated values of the FP coefficients are shown in Fig. 4 for motion within a purely quadrupole potential up to a large amplitude. Although the zero lifetime treatment does not apply to the parameters of our study, we find it instructive to compare the coefficients calculated by using the expressions for zero lifetime with the finite lifetime treatment. For harmonic oscillator motion, the action drift (cooling) rates Π_I^z and Π_I^f nearly coincide in this limit and are given by $\Pi_I^{f,p} \propto -1/\sqrt{I}$ of Eq. (B3), since the correction to the drift coefficient that comes from the spontaneous emission term $\propto \mu$ in Eq. (70), where the zero lifetime and finite lifetime expressions differ, is negligible for these parameters. The diffusion coefficient calculated by Π_{II}^z for a harmonic oscillator can be seen to saturate [Eq. (B5)], while it in fact grows as the amplitude of the motion gets larger [$\Pi_{II}^{f,p} \propto \sqrt{I}$, Eq. (B4)].

For the time-dependent Mathieu oscillator, the action drift rates again nearly coincide within the zero and finite lifetime limits. The diffusion coefficients show a more distinct behavior. The Mathieu oscillator diffusion is much larger than the harmonic oscillator diffusion. In addition, in contrast to the harmonic oscillator case, the large diffusion is predicted by the zero lifetime expressions. This is because the emission occurring at some later time after the absorption [as expressed by the averaging over the decay process, $\langle \cdot \rangle_{\Gamma}$ in Eq. (71)], is no longer the main cause for the large diffusion. Rather, due to the fast micromotion, the absorption and following emission occur at various phase-space points along the trajectory, where the kick to the action (determined by $\partial\Lambda/\partial p_z \propto \pi_c$) can

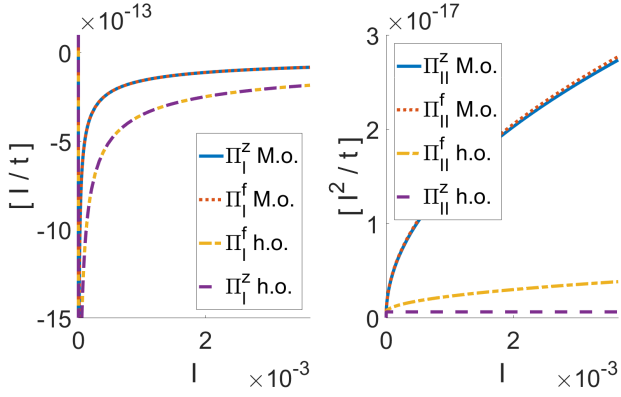


FIG. 4. (a) The action drift and (b) diffusion coefficients in the large amplitude regime within a quadrupole potential, calculated using the expressions of the zero lifetime limit (Π_{II}^z, Π_{II}^z) and the finite lifetime treatment (Π_I^f, Π_{II}^f), with trap and laser parameters given in App. A and Eq. (81). (a) The drift curves calculated (for the harmonic oscillator and separately for the Mathieu oscillator) using the zero lifetime expressions very closely coincide with their values within the finite lifetime treatment. (b) For the harmonic oscillator, the diffusion rate in the zero lifetime limit saturates at a constant value, which quantitatively and qualitatively differs from the results of the finite lifetime treatment. For the Mathieu oscillator the diffusion coefficient calculated using the zero lifetime expression (Π_{II}^z) nearly coincides with the curve for the finite lifetime (Π_{II}^f). See the text for a detailed discussion.

be both positive and negative. Although the average of all kicks remains negative, their variance is much bigger.

As Fig. 4 suggests, although the dynamics within the time-independent potential are simpler than within the time-dependent one, laser cooling with the latter can in some cases be well described using the simpler zero lifetime limit. Formulating a criterion that explicitly states under which circumstances the tori averages of the drift and (in particular) the diffusion coefficients for the finite lifetime limit can be approximated by the zero lifetime limit appears to be hard. However, since the zero lifetime expressions are simpler and faster to calculate numerically, it is worth having this possible shortcut in mind when performing a numerical study of laser cooling based on concrete trap and laser parameters.

Our results allow us to derive a further important conclusion regarding the nature of the cooling. The numerically calculated coefficients show that in the fast particle limit, the asymptotic behaviour within the Mathieu oscillator has the same functional dependence as that within a harmonic oscillator, $\Pi_I^{\text{f.p.}} \propto -1/\sqrt{I}$ and $\Pi_{II}^{\text{f.p.}} \propto \sqrt{I}$, which immediately implies that in this limit, the efficiency coefficient of Eq. (63) is independent of the amplitude, since

$$\varepsilon^{\text{f.p.}}(I) \equiv \frac{\Pi_I^{\text{f.p.}} I}{\Pi_{II}^{\text{f.p.}}} = \text{const} < 0. \quad (83)$$

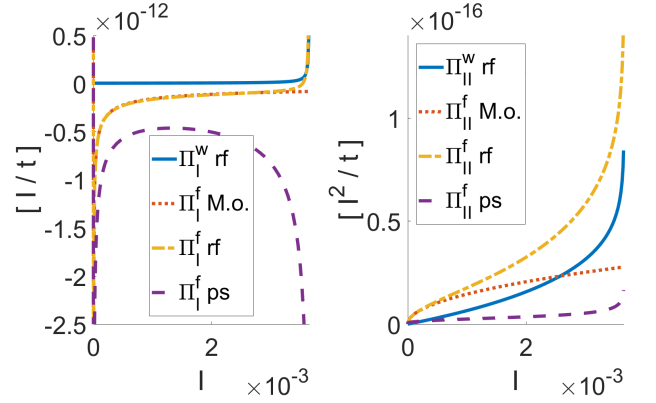


FIG. 5. (a) The action drift and (b) diffusion coefficients for white noise heating and laser cooling within different types of Paul trap potentials. The laser cooling coefficients (Π_I^f for the drift and Π_{II}^f for the diffusion) are compared for motion within a Mathieu oscillator, the surface trap full rf potential, and its pseudopotential approximation. The coefficients of white noise heating (Π_I^w and Π_{II}^w , within the rf potential) are shown as well. The trap and laser parameters are as in Fig. 4, and the heating rate is given in Eq. (82). We note that the I axis here extends to $I = 3.65 \times 10^{-3}$ (where $\nu(I) \approx 0.03$), at the border where the rf potential motion becomes chaotic for the presented parameters). See text for details and a discussion.

We note that in this ratio, the saturation parameter drops out (in our low saturation limit). As long as an appropriate choice of the laser parameters guarantees that $|\varepsilon^{\text{f.p.}}(I)| \gg 1$, the cooling process is efficient (and non-diffusive), independent of the action.

C. Cooling in an anharmonic Paul trap potential

Comparing the cooling coefficients for motion within the surface-electrode trap potential, Fig. 5(a) shows that a calculation using the pseudopotential results in a laser-induced drift rate very different from the rf potential. Cooling within the rf potential is well described by the Mathieu oscillator approximation throughout most of the trap. However, beyond a certain amplitude of motion, the cooling turns into heating as evidenced by the drift coefficient becoming positive. In this region, the corrections to the cooling rate coming from the two terms at order p_r^2 , dominate the drift rate. The heating from white noise corresponding to a heating rate of 0.1 ms^{-1} [Eq. (82)] is shown for comparison, calculated for the motion in the anharmonic potential. Both can be seen to start diverging in the region of motion that approaches the separatrix. This results from the term $\propto \nu^{-3} dI/d\nu$ that enters Π_I^f through $\partial^2 \Lambda / \partial p_z^2$ [Eq. (53)], and becomes important only close enough to the separatrix, although it should be noted that $\nu(I)$ at the maximal value of I in

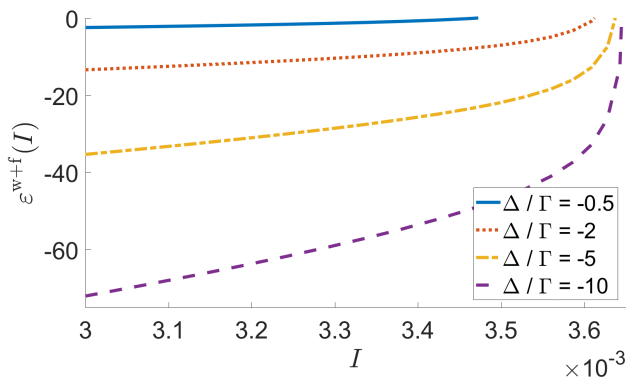


FIG. 6. The cooling efficiency coefficient $\varepsilon^{\text{w+f}}(I)$ of Eq. (85), in the large amplitude regime of a surface-electrode trap. Four values of the detuning Δ are shown, with the rest of the parameters as in Fig. 5. The vertical axis is truncated at $\varepsilon = 0$, beyond which the combined effect of the noise and laser is a mean positive drift. However, already in the range $\varepsilon \gtrsim -1$, the cooling is inefficient, with the diffusion (due to the noise and laser together) dominating the drift, which can quickly lead the ion above the trap's barrier.

Fig. 5 is still $\sim 1/4$ of its value at the trap center, so our adiabatic approximation still holds. The action axis extends up to the maximal value for which a simulation of the full rf potential shows that the ion is still bounded (by the last unbroken torus [11]). For the presented parameters the voltage on the rf electrodes is within the border of validity of the pseudopotential, and the chaotic region close to the separatrix is very small.

The trap anharmonicity plays a bigger role in the diffusion coefficients [Fig. 5(b)]. Here again, the pseudopotential curve is quantitatively very different. Also the approximation of the rf potential by a Mathieu oscillator, results in an underestimate of the action diffusion for nonlinear motion. Turning to the cooling efficiency

$$\varepsilon^{\text{f}}(I) = \frac{\Pi_I^{\text{f}} I}{\Pi_{II}^{\text{f}}}, \quad (84)$$

for low detuning as in Fig. 5 (where $\Delta = -\Gamma/2$) we find that $\varepsilon^{\text{f}}(I) \ll -1$ throughout most of the trap (beyond the very low amplitude motion of thermal equilibrium), and it increases only for very high amplitude motion ($\varepsilon(I) > -1$ for $I \gtrsim 3.5 \times 10^{-3}$). This border is close to (but still lower than) the point where the laser would start heating the ion ($\varepsilon(I) > 0$). The reason that $|\varepsilon(I)|$ becomes of order 1 is inherent to the anharmonic rf potential. As can be seen in Fig. 5, the diffusion grows more steeply than in a quadrupole dependence (for which $\Pi_{II}^{\text{f,P}} \propto \sqrt{I}$), already at values of I where the drift is still close to its quadrupole behaviour. We can conclude that due to the nonlinearity the cooling efficiency strongly decreases with the amplitude, and beyond a certain threshold action, the ion motion under cooling becomes diffusive in nature.

Nonetheless, this threshold can be pushed up by varying other parameters of the cooling [though not the intensity, which cancels out in Eq. (84)]. We find that for a larger detuning the cooling efficiency can be increased. This is clear from, e.g. Eq. (B3), for a quadrupole potential. The action value above which $\varepsilon(I) \gtrsim -1$ (where the motion under cooling becomes diffusive), depends on other parameters of the trap, laser, and on their combined effect together with the white noise. The white noise diffusion coefficient is plotted in Fig. 5(b), for comparison with the laser induced diffusion. For the chosen parameters we see that the laser diffusion is comparable to the noise diffusion for high amplitude motion. The linearity of the FP equation allows us to examine the cooling efficiency in the presence of white noise,

$$\varepsilon^{\text{w+f}}(I) = \frac{(\Pi_I^{\text{w}} + \Pi_I^{\text{f}}) I}{\Pi_{II}^{\text{w}} + \Pi_{II}^{\text{f}}}, \quad (85)$$

presented in Fig. 6. For the lowest value of the detuning, the cooling becomes inefficient already at $I \gtrsim 3.36 \times 10^{-3}$, due to the white noise (however increasing the laser intensity reduces the relative importance of the noise contribution). For increased detuning, the limits of this region can be pushed noticeably up. A detailed study of this regime of high amplitude motion could prove important for optimizing ion loading, and we will examine some aspects of ion dynamics subject to a large laser detuning in [34].

VII. SUMMARY

The main purpose of the current paper has been to lay down a framework for treating stochastic processes in rf traps, throughout the regular parts of the unperturbed Hamiltonian phase-space. In general this requires accounting for the trap's periodic drive and its anharmonicity. This can be achieved by employing action-angle coordinates, which also permit significant simplification of the treatment of slow stochastic processes by integrating over the angles. We have kept the derivations of the theory completely general for 3D motion within these assumptions, which should allow extending our detailed analytic and numerical study for 1D motion, to more spatial dimensions and even to more ions. We begin this section with a summary of the main results.

In Sec. V A we study heating by additive, position-independent Gaussian white noise (modelling fluctuating electric fields). The simplest case is that of a quadrupole potential, where the ion is heated up at a constant rate, which is approximately equal for both the harmonic and the Mathieu oscillator. Studying an anharmonic potential, we find that the drift and diffusion rates significantly increase on the high action tori of the trap and, depending on the parameters, may become comparable with the

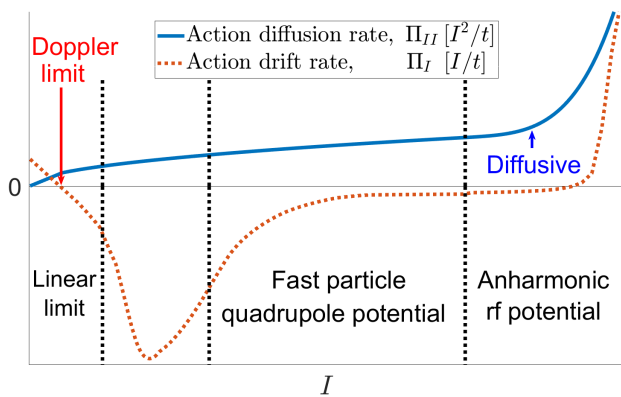


FIG. 7. A schematic depiction of the drift and diffusion rates of the action I , for an ion being laser-cooled in the different regimes of motion within a realistic surface-electrode Paul trap with substantial anharmonicity far away from the effective potential minimum. The axes are not to scale, and the two plotted quantities have different dimensions – see the legend. In the linear limit of the cooling (in the limit of low velocity without “excess micromotion”), the cooling drift and diffusion are linear in the action, and converge to those found for a time-independent trap, with the drift coefficient crossing zero at the action corresponding to the Doppler cooling limit. For high velocity and still within an approximately quadrupole potential, the cooling rate drops as $\propto 1/\sqrt{I}$ and the diffusion rate grows as $\propto \sqrt{I}$. For a very high amplitude of motion within the anharmonic, rf potential, the diffusion grows more sharply and may dominate the drift (so the distribution broadens faster than its mean is cooling down), and the drift itself may become positive (turning into effective heating). In this region the ion is likely to escape the trap, however both effects can be partly remedied by using a large detuning of the cooling beam.

effects of laser cooling.

For laser cooling dynamics, in addition to the degree of the anharmonicity of the potential (that varies with the ion’s displacement from the trap center), a velocity scale determined by the laser parameters is important. When the ion’s velocity is small enough the Lorentzian describing the absorption probability can be linearized in the velocity, while when the ion’s velocity is large enough the ion spends most of its time on the torus within the tails of the Lorentzian. The different regimes of laser cooling are depicted schematically in Fig. 7. For low velocity the cooling coefficients become linear in the action and we find (in Sec. VC and in Sec. VIA) that they nearly coincide for a Mathieu oscillator in this limit with those of the corresponding harmonic oscillator.

For a quantitative measure of the cooling efficiency we define a nondimensional coefficient $\varepsilon(I)$ [in Eq. (63)] proportional to the diffusion timescale divided by the drift timescale. A large negative value of $\varepsilon(I)$ indicates that the ion drifts towards lower action at a rate which overcomes the spread of its probability distribution. For high

velocity motion within a quadrupole potential we find (Sec. VIB) that the cooling efficiency parameter is independent of the action, $\varepsilon(I) = \text{const}$, so the cooling remains effective for any amplitude, if the parameters are chosen to guarantee $\varepsilon \ll -1$.

This simple picture breaks down, however, when the anharmonicity of the potential can no longer be neglected. We find (Sec. VIC) that for a typical low detuning value (optimal for reaching the lowest cooling limit around the trap center), the trap’s anharmonicity in combination with the micromotion lead to diffusive dynamics (dominated by nondirectional diffusion), with $\varepsilon(I) \gtrsim -1$ as the motion amplitude increases within a surface-electrode trap. Moreover, in the very highly anharmonic region close to a separatrix, the drift rate may become positive, with the laser effectively heating the ion past the trap’s boundaries. We also find that a laser detuning much larger than the Doppler detuning allows cooling of the ion from much higher action values.

We can draw general conclusions about the usefulness of the time-independent pseudopotential approximation. As discussed in [11], there exists a regime of parameters where an ion’s motion in a Paul trap is nearly integrable, whence the structure of the phase-space can be well approximated by the pseudopotential, which is simpler to tackle theoretically and to simulate numerically. As we find here, the pseudopotential is also sufficient for a quantitative calculation of white noise heating, where micromotion can be neglected. In contrast, except in its linear limit, laser cooling requires that the micromotion be accounted for even for a quadrupole potential. Moreover, neglecting the micromotion in anharmonic regions within a surface-electrode trap leads to incorrect descriptions of the dynamics. With the (realistic) values of q_z and ν_z stated in Eqs. (A7)-(A8), the pseudopotential approximation fails even for a small micromotion amplitude.

Finally, we note that as discussed in Sec. IIA, we have used an approximate canonical transformation to obtain the rf potential phase-space variables from the pseudopotential ones, simplifying the numerical analysis significantly in the 1D case. This approach neglects corrections of order $\nu(I)^2$, and, as we have verified with a Mathieu oscillator (for which exact analytic expressions are available [33]), amounts to roughly a few percent for our parameters. The frequency $\nu(I)$ and with it the expected inaccuracy only decrease with the amplitude of motion due to anharmonicity in the potential studied here [see Fig. 2(b)], provided that the motion remains nearly integrable. Close enough to a separatrix of the pseudopotential the micromotion introduces chaotic dynamics, posing a natural boundary to the applicability of the presented theory. For the presented parameters the chaos is limited to a very small region of action near the separatrix.

VIII. OUTLOOK

For a study of the stochastic processes of a single ion, the theory can be directly applied in regions of regular motion in those cases where the actions can be calculated. For a quadrupole potential there is no chaotic motion and moreover analytic expressions can be used. If the potential attains a weak anharmonic component, it may be treated perturbatively starting from a quadrupole potential up to some amplitude scale, which makes the calculation feasible [35]. Even for potentials where the anharmonicity is relatively strong (requiring a nonperturbative treatment), there are important cases with a symmetry axis along which the motion nearly decouples from the radial plane [11, 36]. The pseudopotential phase-space for motion in the two radial coordinates is 4D and amenable to an analysis using 2D planar Poincaré surfaces of section, which allow one to calculate the actions. The drift and diffusion coefficients become functions of two variables, which can be readily visualized and analyzed and the micromotion can be accounted for using the canonical transformation employed here. Numerically, one complication in such a study (beyond the tools that have been used in this work and in [11]), could arise from the need to obtain smooth enough maps of phase-space allowing one to take partial derivatives of the actions.

In this work we have focused on a study of the drift and diffusion coefficients and the information that can be extracted directly from them. With different initial conditions, the drift and diffusion coefficients can be used to obtain time-dependent solutions of the FP equation, or to obtain some partial statistics such as the mean time to escape the trap in the absence of cooling, or in contrast, to be cooled to the cooling limit from high amplitude. Our theory can be directly applied to the analysis of Doppler cooling thermometry [20, 23, 37, 38] and related methods [39]. A complex setup can be treated by adding the drift and diffusion coefficients calculated separately for each stochastic process. To account for a spatially inhomogeneous laser profile, the saturation parameter can be generalized to be a function of the coordinates, and the laser parameters can also be modulated in time.

Beyond a single ion, the extension to a crystal of many ions whose motions are linearized about their (periodically driven) equilibrium positions would be immediate using analytic expressions for a coupled Mathieu oscillators system [33, 40], with applications ranging from the cooling of 1D chains of ions [41–48], to planar, 2D and 3D crystals in Paul and also Penning traps [49–55], and applications in quantum information processing [33, 40, 56–73]. The extension of the theory to account for more than two electronic levels could be relevant for different types of ions [23, 74].

In this work we have focused on adiabatic noise heating, typically applicable to electric field fluctuations in

vacuum-operated traps. Collisions of background gas molecules with atomic ions typically induce a nonadiabatic energy change [29, 30, 75], and their separation in time is much larger than the cooling timescale. However, recently objects ranging from large biomolecules, through graphene nanoplatelets to micrometer- and nanometer-scale spheres and diamonds, are being trapped [76–89], and whose dynamics, depending on the pressure in the experiment, can be modelled as Brownian motion. The extension to nonisotropic noise [90] is immediate. Beyond the noise that is inherent to the trap [25, 91–95], it is also possible to introduce forces with differently tailored noise spectra [96, 97] and study the ion’s dynamics or its probability distribution. Such questions stand at the heart of nonequilibrium formulations of reaction-rate theory (Kramer’s escape problem [98]) and stochastic resonances [99]. In combination with laser cooling, a single ion may be captured in a complicated motion [100, 101], and nonequilibrium models of interacting particles coupled to different baths [102–105] could be tested with trapped ions [106], along with various ideas of stochastic, nonequilibrium and active systems.

ACKNOWLEDGMENTS

We thank Vincent Roberdel for very useful discussions. H.L. thanks Giovanna Morigi, Alex Retzker, Shamik Gupta, Anupam Kundu, Oren Raz and Roni Geffen for fruitful discussions. H.L. acknowledges support by a Marie Curie Intra European Fellowship within the 7th European Community Framework Programme, by IRS-IQUPS of Université Paris-Saclay, and by LabEx PALM under grant number ANR-10-LABX-0039-PALM.

Appendix A: Transformation to nondimensional variables and trap parameters

For the numerical calculations presented in this work we use nondimensional units, obtained by rescaling the time t by half the micromotion frequency, $\Omega/2$, and measuring distances using a natural lengthscale of the problem, w , which, for our case, is the electrode width in a five-wire surface-electrode Paul trap [11]). The rescaling introduced in Eq. (46) is,

$$z \rightarrow z/w, \quad t \rightarrow \Omega t/2, \quad v_z \rightarrow v_z/(w\Omega/2). \quad (\text{A1})$$

This rescaling allows us also to use the ion mass m in order to define a nondimensional momentum, and its charge e to define a nondimensional potential energy V that depends on an electrostatic voltage U ,

$$p_z \rightarrow p_z/(mw\Omega/2), \quad U \rightarrow U/[mw^2\Omega^2/(4e)]. \quad (\text{A2})$$

The full potential of the trap can be composed of a sum of a few similar potential terms. The laser parameters are similarly rescaled

$$p_r \rightarrow \frac{p_r}{mw\Omega/2}, \quad \Gamma \rightarrow \frac{\Gamma}{\Omega/2}, \quad \Delta \rightarrow \frac{\Delta}{\Omega/2}, \quad k \rightarrow kw, \quad (\text{A3})$$

in addition to $\omega_L \rightarrow \omega_L/(\Omega/2)$ and $\Omega_R \rightarrow \Omega_R/(\Omega/2)$, together with the rescaled Planck's constant,

$$\hbar \rightarrow \hbar/(mw^2\Omega/2). \quad (\text{A4})$$

For the numerical calculations, we assume throughout this work a ${}^9\text{Be}^+$ ion, and the parameters of Eq. (A1) are

$$w = 50 \mu\text{m} \quad \Omega = 2\pi \times 100 \text{ MHz}. \quad (\text{A5})$$

The other trap parameters are defined by

$$a_z = \frac{4eU_{\text{DC}}/C_z}{mw^2\Omega^2}, \quad q_5 = \frac{2eU_{\text{rf}}}{mw^2\Omega^2}, \quad (\text{A6})$$

with U_{DC} a voltage on electrodes providing confinement along the trap's symmetry axis, C_z is a nondimensional parameter that characterizes the geometric properties of this harmonic potential, and U_{rf} is the voltage on the rf electrodes. The nondimensional parameter values that we choose are

$$q_5 \approx 0.43, \quad a_z = -0.0002, \quad q_z \approx 0.16, \quad (\text{A7})$$

which correspond to $U_{\text{rf}} = 20 \text{ V}$, and this gives

$$\nu_z \approx 0.112, \quad \omega_z \approx 2\pi \times 5.60 \text{ MHz}, \quad (\text{A8})$$

with ω_z the dimensional secular frequency. For the ${}^9\text{Be}^+$ ion, the laser parameters in dimensional units are

$$\tilde{k} \approx 2\pi/313 \text{ nm}^{-1}, \quad \tilde{\Gamma} \approx 120 \times 10^6 \text{ s}^{-1}, \quad (\text{A9})$$

and we take $\vec{k} = k\hat{z}$, with a transverse laser polarization, giving a spontaneous emission coefficient [using Eq. (20)],

$$\mu \equiv \mu_{zz} = 2/5, \quad (\text{A10})$$

(where μ is often denoted by α or ξ in the literature). The nondimensional diffusion coefficient D [after the rescaling of Eq. (46)] is given by

$$D = \frac{8\tilde{D}}{m^2w^2\Omega^3}, \quad (\text{A11})$$

where \tilde{D}/m is the dimensional diffusion coefficient with units of energy increase rate (energy per unit time). Typical measured values are reported as the heating rate \dot{n} in quanta per second (obtained at center of the trap, where the motion can be quantized in terms of a harmonic oscillator). Hence if the oscillator is heated at a rate in dimensional units of $\dot{E} = \hbar\omega_z\dot{n}$, it corresponds to the nondimensional diffusion coefficient,

$$D = \dot{E} = \frac{\hbar}{mw^2} \frac{\omega_z}{(\Omega/2)} \frac{\dot{n}}{(\Omega/2)}. \quad (\text{A12})$$

Appendix B: The fast particle Expansion

Expanding the Lorentzian of Eq. (30) in Δ we get

$$\rho \approx \frac{s}{2} \left[\frac{\Gamma^2}{4(\vec{k} \cdot \vec{v})^2 + \Gamma^2} + \frac{8\vec{k} \cdot \vec{v}\Gamma^2\Delta}{\left(4(\vec{k} \cdot \vec{v})^2 + \Gamma^2\right)^2} \right], \quad (\text{B1})$$

where this expansion is valid for

$$|\vec{k} \cdot \vec{v}| \gg \Gamma/2, \quad |\vec{k} \cdot \vec{v}| \gg 2|\Delta|. \quad (\text{B2})$$

Under the conditions described in Sec. V D (that the laser propagates along $\vec{k} = k\hat{z}$, and if in addition the z motion is described by the harmonic oscillator of Eq. (58)), the conditions in Eq. (B2) are equivalent to Eq. (79), and we can use Eq. (58) to perform the integrals in Eqs. (70)-(71), to get the harmonic oscillator fast particle limit,

$$\Pi_I^{\text{f.p.}} \approx \hbar \frac{\Delta}{\nu_z} \frac{s\Gamma^2/4}{k\sqrt{2I\nu_z}} + \hbar^2 k \frac{s\Gamma^2/4}{2\nu_z\sqrt{2I\nu_z}} (1 + \mu), \quad (\text{B3})$$

$$\Pi_{II}^{\text{f.p.}} \approx \hbar^2 \frac{2(s\Gamma^2/4)}{4\nu_z^2 + \Gamma^2} \left(\frac{\Gamma^3(1 + \mu) + 4\nu_z^2\Gamma}{4\nu_z^2} + \mu k\sqrt{2I\nu_z} \right). \quad (\text{B4})$$

The first term in Eq. (B3) for $\Pi_I^{\text{f.p.}}$ gives cooling (for $\Delta < 0$), and coincides with the result derived for the fast particle limit, using quantum harmonic oscillator wavefunctions, in [15] (where the second term has been neglected). The second term in Eq. (B3) is positive, heating-like, and may counteract the cooling in this asymptotic region of harmonic oscillator motion. Both terms scale with $1/\sqrt{I}$, and the ratio of the second term to the first term of the drift coefficient $\Pi_I^{\text{f.p.}}$, equals $(1 + \mu)kp_r/(2\Delta)$, and for typical parameters (with $|\Delta| \gtrsim \Gamma/2$) this ratio is small by Eq. (24), implying that the positive drift term can be neglected (but not, however, too close to resonance).

The value of $\Pi_{II}^{\text{f.p.}}$ is again the sum of two terms, but these have different asymptotics; the first is constant while the second term scales with \sqrt{I} and gives the dominant functional dependence in the fast particle limit. The latter has the same scaling as that derived in [15] using the quantum harmonic oscillator wavefunctions, however with a different prefactor, consistent with our model of a classical ion [107]. We note for comparison, that the zero lifetime treatment results in the same cooling rate in terms of the energy, but gives a constant diffusion term instead of a term $\propto \sqrt{I}$, which is an *incorrect* result,

$$\Pi_{II}^z \rightarrow \hbar^2 \frac{2(s\Gamma^2/4)\Gamma(1 + \mu)}{4\nu_z^2}, \quad (\text{h.o.}) \quad (\text{B5})$$

This diffusion coefficient can be obtained in the limit of both $\Gamma \gg \nu_z$ and $I \rightarrow 0$ from Eq. (B4), which gives a simple consistency check of the fast particle limit.

Appendix C: Derivatives of the canonical transformation

Using the pseudopotential Hamiltonian,

$$H_{\text{ps}}(\zeta, \pi_\zeta) = \frac{1}{2}\pi_\zeta^2 + V_{\text{ps}}(\zeta), \quad (\text{C1})$$

and the fact that the Hamiltonian becomes angle-independent in the action-angle coordinates, we can write

$$\frac{\partial H_{\text{ps}}(\zeta, \pi_\zeta)}{\partial \pi_\zeta} = \frac{\partial H_{\text{ps}}(I, \theta)}{\partial I} \frac{\partial \Lambda_{\text{ps}}(\zeta, \pi_\zeta)}{\partial \pi_\zeta}. \quad (\text{C2})$$

By rearranging and using the definition of the frequency $\nu(I) = \partial H / \partial I$, we get

$$\frac{\partial \Lambda_{\text{ps}}(\zeta, \pi_\zeta)}{\partial \pi_\zeta} = \frac{\pi_\zeta}{\nu(I)}. \quad (\text{C3})$$

Similarly,

$$\frac{\partial(\pi_\zeta/\nu)}{\partial \pi_\zeta} = \frac{\partial^2 \Lambda_{\text{ps}}(\zeta, \pi_\zeta)}{\partial \pi_\zeta^2} = \frac{1}{\nu} + \pi_\zeta \frac{\partial(1/\nu)}{\partial \pi_\zeta}, \quad (\text{C4})$$

and again,

$$\frac{\partial(1/\nu)}{\partial \pi_\zeta} = \frac{\partial(1/\nu)}{\partial I} \frac{\partial \Lambda_{\text{ps}}}{\partial \pi_\zeta} = -\frac{1}{\nu^2} \frac{d\nu}{dI} \frac{\partial \Lambda_{\text{ps}}}{\partial \pi_\zeta}, \quad (\text{C5})$$

which together with Eqs. (C3)-(C4) allows to obtain Eq. (53) by using Eq. (52) to substitute $\partial/\partial p_z \approx \partial/\partial \pi_\zeta$.

Appendix D: Transformations of the Fokker-Planck equation

We consider a general form of the Fokker-Planck equation for the distribution $\rho(R, P, t)$, written here for 1D case for simplicity, with canonical coordinates $\{R, P\}$,

$$\frac{\partial \rho(R, P, t)}{\partial t} = \mathcal{L}_0(R, P, t)\rho - \sum_{i \in \{R, P\}} \frac{\partial}{\partial i} A_i(R, P, t)\rho + \frac{1}{2} \sum_{i, j \in \{R, P\}} \frac{\partial^2}{\partial i \partial j} B_{ij}(R, P, t)\rho, \quad (\text{D1})$$

where $\mathcal{L}_0(R, P, t)$ is the Liouvillian. For a *canonical* transformation $\{r, p\} = \{\phi_r(R, P, t), \phi_p(R, P, t)\}$, Eq. (D1) transforms to

$$\frac{\partial \rho(r, p, t)}{\partial t} = \mathcal{L}_0(r, p, t)\rho - \sum_{k \in \{r, p\}} \frac{\partial}{\partial k} \tilde{A}_k(r, p, t)\rho + \frac{1}{2} \sum_{k, l \in \{r, p\}} \frac{\partial^2}{\partial k \partial l} \tilde{B}_{kl}(r, p, t)\rho, \quad (\text{D2})$$

where the coefficients \tilde{A}_k and \tilde{B}_{kl} with $k, l \in \{r, p\}$ are given by [108]

$$\tilde{A}_k = \sum_{i \in \{R, P\}} A_i \frac{\partial \phi_k}{\partial i} + \frac{1}{2} \sum_{i, j \in \{R, P\}} B_{ij} \frac{\partial^2 \phi_k}{\partial i \partial j}, \quad \tilde{B}_{kl} = \sum_{i, j \in \{R, P\}} B_{ij} \frac{\partial \phi_k}{\partial i} \frac{\partial \phi_l}{\partial j}, \quad (\text{D3})$$

and we note that the Liouvillian in the new coordinates has to be constructed using the Hamiltonian in the transformed coordinates, $K(r, p, t) = H(r, p, t) + \partial F / \partial t$ with F the generating function of the canonical transformation. More general, time-dependent but noncanonical transformations, and an averaging treatment, are presented in [35].

-
- [1] Wolfgang Paul. Electromagnetic traps for charged and neutral particles. *Reviews of modern physics*, 62(3):531, 1990.
- [2] David J Wineland and Wayne M Itano. Laser cooling of atoms. *Physical Review A*, 20(4):1521, 1979.
- [3] David J. Wineland. Nobel lecture: Superposition, entanglement, and raising schrödinger's cat. *Rev. Mod. Phys.*, 85:1103–1114, Jul 2013.

- [4] C. J. Ballance, T. P. Harty, N. M. Linke, M. A. Sepiol, and D. M. Lucas. High-fidelity quantum logic gates using trapped-ion hyperfine qubits. *Phys. Rev. Lett.*, 117:060504, Aug 2016.
- [5] R. Blatt, P. Zoller, G. Holzmüller, and I. Siemers. Brownian motion of a parametric oscillator: A model for ion confinement in radio frequency traps. *Zeitschrift für Physik D Atoms, Molecules and Clusters*, 4(2):121–126,

- 1986.
- [6] E. Joos and A. Lindner. Langevin equation for the parametric oscillator: a model for ion confinement in a radio frequency trap. *Zeitschrift für Physik D Atoms, Molecules and Clusters*, 11(4):295–300, 1989.
 - [7] VA Alekseev and DD Krylova. Effect of micromotion on the distribution function of ions cooled by laser light in a radiofrequency trap. *JETP LETTERS C/C OF PIS'MA V ZHURNAL EKSPERIMENTAL'NOI TEORETICHESKOI FIZIKI*, 60:5–5, 1994.
 - [8] JR Soběhart and R Farengo. A singular perturbation approach to ion and electron confinement in trapping fields. *Physics of plasmas*, 1(5):1128–1136, 1994.
 - [9] JI Cirac, LJ Garay, R Blatt, AS Parkins, and P Zoller. Laser cooling of trapped ions: The influence of micromotion. *Physical review A*, 49(1):421, 1994.
 - [10] RG DeVoe, J Hoffnagle, and RG Brewer. Role of laser damping in trapped ion crystals. *Physical Review A*, 39(9):4362, 1989.
 - [11] V. Roberdel, D. Leibfried, D. Ullmo, and H. Landa. Phase-space study of surface-electrode paul traps: Integrable, chaotic, and mixed motions. *Phys. Rev. A*, 97:053419, May 2018.
 - [12] Hendrik Anthony Kramers. Brownian motion in a field of force and the diffusion model of chemical reactions. *Physica*, 7(4):284–304, 1940.
 - [13] J. Javanainen. Light-pressure cooling of trapped ions in three dimensions. *Applied Physics*, 23(2):175–182, 10 1980.
 - [14] J. Javanainen and S. Stenholm. Laser cooling of trapped particles i: The heavy particle limit. *Applied Physics*, 21(3):283–291, 03 1980.
 - [15] Juha Javanainen and Stig Stenholm. Laser cooling of trapped particles ii. *Applied Physics A: Materials Science & Processing*, 24(1):71–84, 1981.
 - [16] JP Gordon and A Ashkin. Motion of atoms in a radiation trap. *Physical Review A*, 21(5):1606, 1980.
 - [17] Stig Stenholm. The semiclassical theory of laser cooling. *Reviews of modern physics*, 58(3):699, 1986.
 - [18] Marek Šašura and Vladimír Bužek. Cold trapped ions as quantum information processors. *journal of modern optics*, 49(10):1593–1647, 2002.
 - [19] D. Leibfried, R. Blatt, C. Monroe, and D. Wineland. Quantum dynamics of single trapped ions. *Reviews of Modern Physics*, 75(1):281–324, 2003.
 - [20] J. H. Wesenberg, R. J. Epstein, D. Leibfried, R. B. Blakestad, J. Britton, J. P. Home, W. M. Itano, J. D. Jost, E. Knill, C. Langer, R. Ozeri, S. Seidelin, and D. J. Wineland. Fluorescence during doppler cooling of a single trapped atom. *Physical Review A*, 76(5), 11 2007.
 - [21] R. J. Epstein, S. Seidelin, D. Leibfried, J. H. Wesenberg, J. J. Bollinger, J. M. Amini, R. B. Blakestad, J. Britton, J. P. Home, W. M. Itano, J. D. Jost, E. Knill, C. Langer, R. Ozeri, N. Shiga, and D. J. Wineland. Simplified motional heating rate measurements of trapped ions. *Physical Review A*, 76(3), 09 2007.
 - [22] M. Marciantie, C. Champenois, A. Calisti, J. Pedregosa-Gutierrez, and M. Knoop. Ion dynamics in a linear radio-frequency trap with a single cooling laser. *Physical Review A*, 82(3), 09 2010.
 - [23] Tomas Sikorsky, Ziv Meir, Nitzan Akerman, Ruti Ben-shlomi, and Roei Ozeri. Doppler cooling thermometry of a multilevel ion in the presence of micromotion. *Phys. Rev. A*, 96:012519, Jul 2017.
 - [24] M. Brownnutt, M. Kumph, P. Rabl, and R. Blatt. Ion-trap measurements of electric-field noise near surfaces. *Reviews of Modern Physics*, 87(4):1419–1482, 12 2015.
 - [25] Q. A. Turchette, Kielpinski, B. E. King, D. Leibfried, D. M. Meekhof, C. J. Myatt, M. A. Rowe, C. A. Sackett, C. S. Wood, W. M. Itano, C. Monroe, and D. J. Wineland. Heating of trapped ions from the quantum ground state. *Physical Review A*, 61(6), 05 2000.
 - [26] C. D. Bruzewicz, J. M. Sage, and J. Chiaverini. Measurement of ion motional heating rates over a range of trap frequencies and temperatures. *Physical Review A*, 91(4), 04 2015.
 - [27] JA Sedlacek, A Greene, J Stuart, R McConnell, CD Bruzewicz, JM Sage, and J Chiaverini. Distance scaling of electric-field noise in a surface-electrode ion trap. *arXiv preprint arXiv:1712.00188*, 2017.
 - [28] N.G. Van Kampen. *Stochastic processes in physics and chemistry*. Elsevier Science, United States, 3 edition, 03 2007.
 - [29] Ralph G DeVoe. Power-law distributions for a trapped ion interacting with a classical buffer gas. *Physical review letters*, 102(6):063001, 2009.
 - [30] I Rouse and S Willitsch. Superstatistical energy distributions of an ion in an ultracold buffer gas. *Physical review letters*, 118(14):143401, 2017.
 - [31] H. Landa. Tuning nonthermal distributions to thermal ones in time-dependent Paul traps. *arXiv preprint arXiv:1809.10519*, 2018.
 - [32] see Chapter VIII of [28].
 - [33] H Landa, M Drewsen, B Reznik, and A Retzker. Classical and quantum modes of coupled mathieu equations. *Journal of Physics A: Mathematical and Theoretical*, 45(45):455305, 2012.
 - [34] A. Maitra, D. Leibfried, D. Ullmo, and H. Landa. Can a periodically driven particle resist laser cooling and noise? *arXiv preprint arXiv:1810.01856*, 2018.
 - [35] Sreedhar B. Dutta and Mustansir Barma. Asymptotic distributions of periodically driven stochastic systems. *Phys. Rev. E*, 67:061111, Jun 2003.
 - [36] Andrew C Wilson, Yves Colombe, Kenton R Brown, Emanuel Knill, Dietrich Leibfried, and David J Wineland. Tunable spin–spin interactions and entanglement of ions in separate potential wells. *Nature*, 512(7512):57, 2014.
 - [37] Thomas Lauprêtre, Rasmus B Linnet, Ian D Leroux, Haggai Landa, Aurélien Dantan, and Michael Drewsen. Controlling the potential landscape and normal modes of ion coulomb crystals by a standing-wave optical potential. *Physical Review A*, 99(3):031401, 2019.
 - [38] Ziv Meir, Meirav Pinkas, Tomas Sikorsky, Ruti Ben-shlomi, Nitzan Akerman, and Roei Ozeri. Direct observation of atom-ion non-equilibrium sympathetic cooling. *arXiv preprint arXiv:1801.06839*, 2018.
 - [39] Craig R Clark, James E Goeders, Yatis K Dodia, C Riccardo Viteri, and Kenneth R Brown. Detection of single-ion spectra by coulomb-crystal heating. *Physical Review A*, 81(4):043428, 2010.

- [40] H. Landa, M. Drewsen, B. Reznik, and A. Retzker. Modes of oscillation in radiofrequency Paul traps. *New Journal of Physics*, 14(9):093023, 2012.
- [41] Giovanna Morigi and Jürgen Eschner. Doppler cooling of a coulomb crystal. *Phys. Rev. A*, 64:063407, Nov 2001.
- [42] Giovanna Morigi and Jürgen Eschner. Is an ion string laser-cooled like a single ion? *Journal of Physics B: Atomic, Molecular and Optical Physics*, 36(5):1041, 2003.
- [43] G. Morigi and H. Walther. Two-species coulomb chains for quantum information. *The European Physical Journal D-Atomic, Molecular, Optical and Plasma Physics*, 13(2):261–269, 2001.
- [44] Thomás Fogarty, Haggai Landa, Cecilia Cormick, and Giovanna Morigi. Optomechanical many-body cooling to the ground state using frustration. *Physical Review A*, 94(2):023844, 2016.
- [45] Marius Romuald Kamsap, Caroline Champenois, J Pedregosa-Gutierrez, Simon Mahler, Marie Houssin, and Martina Knoop. Experimental demonstration of an efficient number diagnostic for long ion chains. *Physical Review A*, 95(1):013413, 2017.
- [46] S. Ejtemaee and P. C. Haljan. 3d sisyphus cooling of trapped ions. *Phys. Rev. Lett.*, 119:043001, Jul 2017.
- [47] Cecilia Cormick, Tobias Schaetz, and Giovanna Morigi. Trapping ions with lasers. *New Journal of Physics*, 13(4):043019, 2011.
- [48] Julian Schmidt, Alexander Lambrecht, Pascal Weckesser, Markus Debatin, Leon Karpa, and Tobias Schaetz. Optical trapping of ion coulomb crystals. *Phys. Rev. X*, 8:021028, May 2018.
- [49] T. B. Mitchell, J. J. Bollinger, D. H. E. Dubin, X.-P. Huang, W. M. Itano, and R. H. Baughman. Direct observations of structural phase transitions in planar crystallized ion plasmas. *Science*, 282(5392):1290–1293, 1998.
- [50] A. Mortensen, E. Nielsen, T. Matthey, and M. Drewsen. Observation of three-dimensional long-range order in small ion coulomb crystals in an rf trap. *Phys. Rev. Lett.*, 96(10):103001, Mar 2006.
- [51] A. Ostendorf, C. B. Zhang, M. A. Wilson, D. Offenberg, B. Roth, and S. Schiller. Sympathetic cooling of complex molecular ions to millikelvin temperatures. *Phys. Rev. Lett.*, 97:243005, Dec 2006.
- [52] B Szymanski, R Dubessy, B Dubost, S Guibal, J-P Likhforman, and L Guidoni. Large two dimensional coulomb crystals in a radio frequency surface ion trap. *Applied Physics Letters*, 100(17):171110, 2012.
- [53] DA Tabor, V Rajagopal, Y-W Lin, and B Odom. Suitability of linear quadrupole ion traps for large coulomb crystals. *Applied Physics B*, 107(4):1097–1104, 2012.
- [54] Sandeep Mavadia, Joseph F Goodwin, Graham Stutter, Shailen Bharadia, Daniel R Crick, Daniel M Segal, and Richard C Thompson. Control of the conformations of ion coulomb crystals in a penning trap. *Nature communications*, 4:2571, 2013.
- [55] Justin G Bohnet, Brian C Sawyer, Joseph W Britton, Michael L Wall, Ana Maria Rey, Michael Foss-Feig, and John J Bollinger. Quantum spin dynamics and entanglement generation with hundreds of trapped ions. *Science*, 352(6291):1297–1301, 2016.
- [56] Q. A. Turchette, C. S. Wood, B. E. King, C. J. Myatt, D. Leibfried, W. M. Itano, C. Monroe, and D. J. Wineland. Deterministic entanglement of two trapped ions. *Phys. Rev. Lett.*, 81:3631–3634, Oct 1998.
- [57] DJ Berkeland, JD Miller, James C Bergquist, Wayne M Itano, and David J Wineland. Minimization of ion micromotion in a paul trap. *Journal of applied physics*, 83(10):5025–5033, 1998.
- [58] A. Retzker, R. C. Thompson, D. M. Segal, and M. B. Plenio. Double well potentials and quantum phase transitions in ion traps. *Phys. Rev. Lett.*, 101:260504, Dec 2008.
- [59] H. Kaufmann, S. Ulm, G. Jacob, U. Poschinger, H. Landa, A. Retzker, M. B. Plenio, and F. Schmidt-Kaler. Precise experimental investigation of eigenmodes in a planar ion crystal. *Phys. Rev. Lett.*, 109:263003, Dec 2012.
- [60] H. Landa, A. Retzker, T. Schaetz, and B. Reznik. Entanglement Generation Using Discrete Solitons in Coulomb Crystals. *Phys. Rev. Lett.*, 113:053001, 2014.
- [61] C. Shen and L.-M. Duan. High-fidelity quantum gates for trapped ions under micromotion. *Phys. Rev. A*, 90:022332, Aug 2014.
- [62] S-T Wang, Chao Shen, and L-M Duan. Quantum computation under micromotion in a planar ion crystal. *Scientific reports*, 5:8555, 2015.
- [63] Kyle Arnold, Elnur Hajiyev, Eduardo Paez, Chern Hui Lee, MD Barrett, and John Bollinger. Prospects for atomic clocks based on large ion crystals. *Physical Review A*, 92(3):032108, 2015.
- [64] J Keller, HL Partner, T Burgermeister, and TE Mehlstäubler. Precise determination of micromotion for trapped-ion optical clocks. *Journal of Applied Physics*, 118(10):104501, 2015.
- [65] LL Yan, W Wan, L Chen, F Zhou, SJ Gong, X Tong, and M Feng. Exploring structural phase transitions of ion crystals. *Scientific reports*, 6:21547, 2016.
- [66] Manuel Mielenz, Henning Kalis, Matthias Wittemer, Frederick Hakelberg, Ulrich Warring, Roman Schmied, Matthew Blain, Peter Maunz, David L Moehring, Dietrich Leibfried, et al. Arrays of individually controlled ions suitable for two-dimensional quantum simulations. *Nature communications*, 7:ncomms11839, 2016.
- [67] Colin D Bruzewicz, Robert McConnell, John Chiaverini, and Jeremy M Sage. Scalable loading of a two-dimensional trapped-ion array. *Nature communications*, 7:13005, 2016.
- [68] Bogdan M Mihalcea. Study of quasiclassical dynamics of trapped ions using the coherent state formalism and associated algebraic groups. *Romanian Journal of Physics*, 62:113, 2017.
- [69] J Keller, D Kalincev, T Burgermeister, A Kulosa, A Didier, T Nordmann, J Kiethe, and TE Mehlstäubler. Optical clocks based on linear ion chains with high stability and accuracy. *arXiv preprint arXiv:1712.02335*, 2017.
- [70] J Keller, T Burgermeister, D Kalincev, A Didier, AP Kulosa, T Nordmann, J Kiethe, and TE Mehlstäubler. Controlling systematic frequency uncertainties at the 10^{-19} level in linear coulomb crystals. *arXiv preprint arXiv:1803.08248*, 2018.

- [71] J Welzel, F Stopp, and F Schmidt-Kaler. Spin and motion dynamics with zigzag ion crystals in transverse magnetic field gradients. *arXiv preprint arXiv:1801.03391*, 2018.
- [72] Marion Delehaye and Clément Lacroûte. Single-ion, transportable optical atomic clocks. *Journal of Modern Optics*, 65(5-6):622–639, 2018.
- [73] Yukai Wu, Sheng-Tao Wang, and L.-M. Duan. Noise analysis for high-fidelity quantum entangling gates in an anharmonic linear paul trap. *Phys. Rev. A*, 97:062325, Jun 2018.
- [74] H Janacek, AM Steane, DM Lucas, and DN Stacey. The effect of atomic response time in the theory of doppler cooling of trapped ions. *Journal of Modern Optics*, 65(5-6):577–584, 2018.
- [75] I Rouse and S Willitsch. Energy distributions of an ion in a radio-frequency trap immersed in a buffer gas under the influence of additional external forces. *Physical Review A*, 97(4):042712, 2018.
- [76] D Offenber, CB Zhang, Ch Wellers, B Roth, and S Schiller. Translational cooling and storage of protonated proteins in an ion trap at subkelvin temperatures. *Physical Review A*, 78(6):061401, 2008.
- [77] J. Millen, P. Z. G. Fonseca, T. Mavrogordatos, T. S. Monteiro, and P. F. Barker. Cavity cooling a single charged levitated nanosphere. *Phys. Rev. Lett.*, 114:123602, Mar 2015.
- [78] Daniel Goldwater, Mauro Paternostro, and P. F. Barker. Testing wave-function-collapse models using parametric heating of a trapped nanosphere. *Phys. Rev. A*, 94:010104, Jul 2016.
- [79] I. Alda, J. Berthelot, R. A. Rica, and R. Quidant. Trapping and manipulation of individual nanoparticles in a planar paul trap. *Applied Physics Letters*, 109(16):163105, 2016.
- [80] B. E. Kane. Levitated spinning graphene flakes in an electric quadrupole ion trap. *Phys. Rev. B*, 82:115441, Sep 2010.
- [81] Bogdan M Mihalcea, Liviu C Giurgiu, Cristina Stan, Gina T Vişan, Mihai Ganciu, Vladimir Filinov, Dmitry Lapitsky, Lidiya Deputatova, and Roman Syrovatka. Multipole electrodynamic ion trap geometries for microparticle confinement under standard ambient temperature and pressure conditions. *Journal of Applied Physics*, 119(11):114303, 2016.
- [82] Pavel Nagornykh, Joyce E Coppock, and BE Kane. Cooling of levitated graphene nanoplatelets in high vacuum. *Applied Physics Letters*, 106(24):244102, 2015.
- [83] P. Z. G. Fonseca, E. B. Aranas, J. Millen, T. S. Monteiro, and P. F. Barker. Nonlinear dynamics and strong cavity cooling of levitated nanoparticles. *Phys. Rev. Lett.*, 117:173602, Oct 2016.
- [84] Irene Alda, Johann Berthelot, Raúl A Rica, and Romain Quidant. Trapping and manipulation of individual nanoparticles in a planar paul trap. *Applied Physics Letters*, 109(16):163105, 2016.
- [85] EB Aranas, PZG Fonseca, PF Barker, and TS Monteiro. Thermometry of levitated nanoparticles in a hybrid electro-optical trap. *Journal of Optics*, 19(3):034003, 2017.
- [86] Heather L Partner, Joachim Zoll, Alexander Kuhlicke, and Oliver Benson. Printed-circuit-board linear paul trap for manipulating single nano-and microparticles. *Review of Scientific Instruments*, 89(8):083101, 2018.
- [87] Tom Delord, Louis Nicolas, Lucien Schwab, and Gabriel Hétet. Electron spin resonance from nv centers in diamonds levitating in an ion trap. *arXiv preprint arXiv:1605.02953*, 2016.
- [88] T Delord, L Nicolas, M Bodini, and G Hétet. Diamonds levitating in a paul trap under vacuum: measurements of laser-induced heating via nv center thermometry. *arXiv preprint arXiv:1701.06407*, 2017.
- [89] T Delord, L Nicolas, Y Chassagneux, and G Hétet. Strong coupling between a single nv spin and the torsional mode of diamonds levitating in an ion trap. *arXiv preprint arXiv:1702.00774*, 2017.
- [90] Philipp Schindler, Dylan J Gorman, Nikos Daniilidis, and Hartmut Häffner. Polarization of electric-field noise near metallic surfaces. *Phys. Rev. A*, 92:013414, Jul 2015.
- [91] N Daniilidis, S Narayanan, S A Mller, R Clark, T E Lee, P J Leek, A Wallraff, St Schulz, F Schmidt-Kaler, and H Haeffner. Fabrication and heating rate study of microscopic surface electrode ion traps. *New Journal of Physics*, 13(1):013032, 2011.
- [92] N. Daniilidis, S. Gerber, G. Bolloten, M. Ramm, A. Ransford, E. Ulin-Avila, I. Talukdar, and H. Häffner. Surface noise analysis using a single-ion sensor. *Phys. Rev. B*, 89:245435, Jun 2014.
- [93] M Brownnutt, M Kumph, P Rabl, and R Blatt. Ion-trap measurements of electric-field noise near surfaces. *Reviews of Modern Physics*, 87(4):1419, 2015.
- [94] Peter A Ivanov, Nikolay V Vitanov, and Kilian Singer. High-precision force sensing using a single trapped ion. *Scientific reports*, 6:28078, 2016.
- [95] K Lakhmanskii, PC Holz, D Schärfl, B Ames, R Assouly, T Monz, Y Colombe, and R Blatt. Observation of superconductivity and surface noise using a single trapped ion as a field probe. *arXiv preprint arXiv:1805.00793*, 2018.
- [96] J. A. Sedlacek, A. Greene, J. Stuart, R. McConnell, C. D. Bruzewicz, J. M. Sage, and J. Chiaverini. Distance scaling of electric-field noise in a surface-electrode ion trap. *Phys. Rev. A*, 97:020302, Feb 2018.
- [97] JA Sedlacek, J Stuart, W Loh, R McConnell, CD Bruzewicz, JM Sage, and J Chiaverini. Method for determination of technical noise contributions to ion motional heating. *arXiv preprint arXiv:1805.09491*, 2018.
- [98] Peter Hänggi, Peter Talkner, and Michal Borkovec. Reaction-rate theory: fifty years after Kramers. *Reviews of modern physics*, 62(2):251, 1990.
- [99] Luca Gammaitoni, Peter Hänggi, Peter Jung, and Fabio Marchesoni. Stochastic resonance. *Reviews of modern physics*, 70(1):223, 1998.
- [100] A. E. Kaplan. Single-particle motional oscillator powered by laser. *Opt. Express*, 17(12):10035–10043, Jun 2009.
- [101] N. Akerman, S. Kotler, Y. Glickman, Y. Dallal, A. Kesselman, and R. Ozeri. Single-ion nonlinear mechanical oscillator. *Phys. Rev. A*, 82:061402, Dec 2010.
- [102] Victor Dotsenko, Anna Maciołek, Oleg Vasilyev, and

- Gleb Oshanin. Two-temperature langevin dynamics in a parabolic potential. *Physical Review E*, 87(6):062130, 2013.
- [103] AY Grosberg and J-F Joanny. Nonequilibrium statistical mechanics of mixtures of particles in contact with different thermostats. *Phys. Rev. E*, 92(3):032118, 2015.
- [104] Simon N Weber, Christoph A Weber, and Erwin Frey. Binary mixtures of particles with different diffusivities demix. *Physical review letters*, 116(5):058301, 2016.
- [105] Vincent Mancois, Bruno Marcos, Pascal Viot, and David Wilkowski. Two-temperature brownian dynamics of a particle in a confining potential. *arXiv preprint arXiv:1802.04584*, 2018.
- [106] J Brox, P Kiefer, M Bujak, T Schaetz, and H Landa. Spectroscopy and directed transport of topological solitons in crystals of trapped ions. *Physical review letters*, 119(15):153602, 2017.
- [107] To relate the notation of [15] to our variables, $\mu = 1/3$, $N = k\sqrt{2I\nu}/\nu$, and $2\kappa^2 = s\Gamma^2/4$. Our result for $\Pi_{II}^{\text{f.p.}}$ is smaller by the factor $4\nu_z^2/(\Gamma^2 + 4\nu_z^2)$. In [15] it is argued that due to the form of the quantum wavefunctions of the harmonic oscillator, the ion's emission peaks at maximum momentum. This argument does not apply to our model, obtained by assuming a localized ion, oscillating in the trap with well-defined phase-space coordinates.
- [108] See page 286 of [28].